PAPER

Biofunctionalization of electrospun silk scaffolds with perlecan for vascular tissue engineering†

Shouyuan Jiang,‡[a] Anyu Zhang,[b] Behnam Akhavan, [b,c,d,e] John Whitelock,[a] Marcela M. Bilek,[b,c,d,f] Steven G. Wise, [d,f,g] Megan S. Lord [*a,h] and Jelena Rnjak-Kovacina [*a]

Electrospun silk fibroin scaffolds have garnered significant interest in vascular tissue engineering due to their biocompatibility, mechanical strength, and tunable degradation. However, their lack of intrinsic cell-binding domains limits endothelialization, a critical factor for vascular graft success. This study explores the biofunctionalization of electrospun silk scaffolds with recombinant perlecan domain V (rDV) using plasma immersion ion implantation (PIII) treatment, a surface modification method enabling robust covalent immobilization without the use of reagents. The biofunctionalized scaffolds enhanced endothelial cell adhesion, proliferation, and retention under physiological flow conditions while inhibiting smooth muscle cell proliferation. Additionally, the functionalized scaffolds demonstrated angiogenic potential *in vivo*. These findings underscore the potential of rDV-functionalized silk scaffolds as a promising candidate for small-diameter vascular grafts, addressing key challenges of endothelialization and vascular cell modulation in clinical applications.

1. Introduction

Cardiovascular disease is the leading cause of death globally, primarily driven by atherosclerosis—a chronic inflammatory condition characterized by lipid accumulation, vessel wall thickening, and stenosis.[1,2] While lifestyle changes and lipid-lowering therapies are first-line treatments, advanced cases often require surgical interventions like angioplasty with stenting or bypass surgery.[3] For severe blockages such as in the coronary artery, bypass surgery using autologous vessels is preferred, but nearly half of patients lack suitable donor vessels due to factors like age or prior surgeries.[4–6] Synthetic grafts,

effective in large-diameter applications, show poor long-term patency in small-diameter vessels (<6 mm), highlighting the need for improved alternatives.[7,8]

The use of *Bombyx mori* silk fibroin (silk) in vascular tissue engineering has emerged as a promising strategy due to its excellent mechanical properties, cytocompatibility, and tunable biodegradability to match the rate of vascular tissue regeneration.[9–12] Electrospun silk grafts in particular, offer a nanofibrous structure that mimics the native extracellular matrix (ECM), promoting cell adhesion, migration, and tissue integration.[13–15] These scaffolds can be engineered to possess mechanical properties comparable to native arteries and outperform conventional expanded polytetrafluoroethylene (ePTFE) grafts in a preclinical model[13] and were shown to remodel with native collagen and elastin *in vivo*.[14] Additionally, electrospinning enables precise control over fiber diameter, alignment, and porosity,[16,17] which is essential for optimizing graft mechanics and degradation profiles. However, limited endothelialization remains a critical barrier to the successful clinical application of silk-based vascular grafts, as the lack of inherent cell-binding domains restricts effective endothelial cell attachment and proliferation.[18] Biofunctionalization of electrospun silk conduits with endothelial cell interacting moieties may enhance graft endothelialization.

Recombinantly expressed domain V (rDV) of human perlecan (heparan sulfate proteoglycan, HSPG2; a key component of the vascular basement membrane and a molecule essential in

[a]*Graduate School of Biomedical Engineering, University of New South Wales, Sydney, NSW 2052, Australia. E-mail: j.rnjak-kovacina@unsw.edu.au; Tel: +61 2 9385 3920*
[b]*School of Biomedical Engineering, The University of Sydney, Sydney, NSW 2006, Australia*
[c]*School of Physics, The University of Sydney, Sydney, Australia*
[d]*The University of Sydney Nano Institute, University of Sydney, Sydney, NSW 2006, Australia*
[e]*School of Engineering, University of Newcastle, Callaghan, NSW 2308, Australia*
[f]*Charles Perkins Centre, The University of Sydney, Sydney, Australia*
[g]*School of Medical Sciences, Faculty of Health and Medicine, University of Sydney, Sydney, NSW 2006, Australia*
[h]*UNSW RNA Institute, University of New South Wales, Sydney, NSW 2052, Australia. E-mail: m.lord@unsw.edu.au; Tel: +61 2 9385 3910*

vascular development and homeostasis) enhances endothelial cell adhesion (*via* the $\alpha_2\beta_1$ integrin binding site), proliferation, and migration, which are key steps to the formation of vascular graft endothelium.[18–20] Further, rDV was shown to interact with endogenous angiogenic growth factors through its glycosaminoglycan (GAG) chains and promote angiogenesis, which is important for graft integration and transmural capillarization.[19,21] This and its ability to inhibit smooth muscle cell proliferation and platelet adhesion demonstrated in previous studies,[22,23] make rDV an attractive bioactive molecule for the biofunctionalization of electrospun silk vascular grafts.

Passive adsorption is a simple approach to immobilize molecules on silk materials, and rDV biofunctionalized electrospun silk was shown to promote graft endothelialization in a mouse carotid interposition model.[21] However, non-specific adsorption often results in weak bonds that are easily displaced when placed in dynamic biological environments such as the blood vessels.[18] Covalent immobilization on silk can be achieved *via* 1-ethyl-3-(3-dimethylaminopropyl)carbodiimide/*N*-hydrosuccinimide (EDC/NHS) chemistry which results in the formation of an amide bond.[9] Immobilization of rDV on silk films *via* EDC/NHS results in improved presentation of the rDV $\alpha_2\beta_1$ integrin binding site to endothelial cells, which led to enhanced endothelial cell adhesion, spreading, and proliferation relative to that on passively adsorbed rDV.[18] However, this technique relies on biofunctionalization *via* low abundance aspartic (0.5 mol% in silk) and glutamic (0.6 mol% in silk) amino acids in silk.[9] In contrast, plasma immersion ion implantation (PIII) treatment is a reagent-free surface modification technique which utilizes high energy ions to break bonds in the material, resulting in the formation of a subsurface layer containing long-lived radicals that facilitate the covalent immobilization of biologically active molecules once they come in contact with the surface.[24] The unpaired electrons associated with embedded radicals migrate to the surface through a series of thermally activated bond abstraction processes.[25] On arrival at the surface, the unpaired electrons can undergo chemical reactions even after a year post-treatment. Unlike conventional covalent immobilization techniques such as EDC/NHS chemistry, which specifically target carboxyl and amine groups, PIII-induced immobilization does not rely on any particular functional groups within the polymer chain.[26] rDV has been successfully immobilized on silk films *via* the PIII treatment with the C-terminal region of rDV more exposed.[27] This region is particularly important as it contains glycosaminoglycan (GAG) attachment sites and integrin-binding domains which support the formation of functional endothelium *in vitro*[27] and support excellent blood compatibility in *ex vivo* studies.[23] However, these fundamental studies were conducted on simple, 2D silk films, which differ significantly in surface topography, mechanical properties, and clinical applicability from the clinically relevant 3D electrospun silk scaffolds used in this study. Electrospun silk presents a highly porous, nanofibrous architecture that that closely mimics the extracellular matrix with increased surface roughness, fiber curvature and porosity that may influence PIII-mediated functionalization and protein immobilization compared to flat silk films, necessitating further investigation. Additionally, the mechanical and hemodynamic properties of electrospun silk differ from silk films, requiring evaluation under physiological and dynamic flow conditions relevant to vascular grafts.

By translating PIII treatment and rDV immobilization to 3D electrospun silk conduits, this study aims to bridge the gap between *in vitro* endothelialization studies on flat substrates and the development of biofunctionalized vascular grafts for clinical applications. Therefore, the potential of electrospun silk scaffolds biofunctionalized with rDV using PIII treatment toward vascular graft applications was explored in this paper. This was achieved by examining how rDV functionalized electrospun silk scaffolds influence endothelial and smooth muscle cell interactions in 2D and 3D cell cultures *in vitro*, and their role in supporting angiogenesis *in vivo*.

2. Materials and methods

All reagents were purchased from Sigma-Aldrich (Castle Hill, Australia) unless stated otherwise.

2.1. rDV expression and purification

Domain V of human perlecan (rDV) was expressed by transfected human embryonic kidney-293 (HEK-293; Cellbank Australia) cells as described previously.[28] Briefly, domain V DNA (2446 bp, exons 79–97) was amplified from human coronary artery endothelial cell (HCAEC) mRNA, cloned into CEFLsec vector with a BM40 signal peptide and transfected into HEK-293 cells using Lipofectamine 2000 transfection reagent (Thermo Fisher Scientific). Stably transfected HEK-293 cells were selected using Geneticin and cultured in Dulbecco's Modified Eagle Medium (DMEM) high glucose with 10% (v/v) fetal bovine serum (Bovogen Biologicals) and 1% (v/v) penicillin–streptomycin. Conditioned medium was routinely collected every 3–4 days and passaged once a week. Conditioned medium from the cultures was purified *via* anion exchange chromatography using a diethylaminoethyl matrix (20 mL, DEAE Sepharose) and purified samples were analyzed for protein concentration through the Bradford protein assay as described previously.[21]

2.2. Silk fibroin solution preparation

Bombyx mori silk cocoons (Tajima Shoji Co. Ltd) were boiled in sodium carbonate solution (in batches of 5 g of silk cocoon per 2 L of 0.02 M sodium carbonate solution) for 30 min and thoroughly washed under running water and dried. Silk fibers were dissolved in lithium bromide (9.3 M, 4 mL g^{-1} silk fibers) at 60 °C for 4 h, and the solution was dialyzed against water using 3500 molecular weight cut-off SnakeSkin dialysis tubing (Life Technologies) for 3 days. Debris was removed by centrifuging at 8700 rpm at 4 °C for 20 min twice. The concentration

of the silk fibroin solution was determined *via* gravimetric analysis, and the silk solution was stored at 4 °C for later use.

2.3. Electrospun silk scaffold fabrication

Electrospinning of the silk fibroin solution was performed with the addition of polyethylene oxide (PEO) as described previously.[13] Briefly, 5% w/v PEO solution (1 g) was added to 8% w/v silk solution (2 mL) and gently mixed on a vertical rotating mixer for 20 min. The mixed solution was then loaded into a syringe (10 mL, Terumo) and pumped at 0.7 mL h^{-1} through a 0.6 mm inner diameter blunted ended needle in the electrospinner (IME technologies), which was subjected to a 15 kV voltage and positively charged. Silk mats were spun on a 20 mm diameter mandrel and silk tubes were spun on a 6 mm diameter mandrel. Mandrels were negatively charged and positioned 18 cm away from the needle tip, rotating at 500 rpm to collect the fibres shooting out of the needle. The silk/PEO mixture was used to spin mats (4 mL) and tubes (2.8 mL). A syringe pump (Harvard Apparatus, Holliston, MA, USA) was used to control the flow rate. Humidity in the electrospinner was maintained between 25–35% using dry ice. Crosslinking of the electrospun silk mats and tubes was performed in a humidified chamber (Wheaton) under vacuum at room temperature overnight. Scaffolds were soaked in water for 3 days with water changes to leach out the PEO, followed by soaking in 70% ethanol for 2 h for sterilization. Scaffolds were rinsed in sterile PBS 4 times and air-dried before storage. The silk mats were created by cutting open the 20 mm diameter electrospun silk tubes to form an electrospun silk sheet. Circular disks (6 mm diameter) were then prepared using a biopsy punch (Livingstone). For 3D cell cultures, 6 mm diameter electrospun silk tube scaffolds were utilized.

2.4. Biofunctionalization of silk scaffolds with rDV

Passive adsorption. For the 6 mm circular silk disks, samples were placed in a 96-well tissue culture plate and rDV solution (50 μL, 50 μg mL^{-1}) was pipetted on each sample and incubated at 37 °C for 2 h. Coated samples were rinsed twice with PBS before further experimentation. For tubular silk scaffolds, silk grafts (2 cm in length) were filled with rDV solution (500 μL, 50 μg mL^{-1}) and sealed using a syringe on each end. The setup was incubated for 2 h at 37 °C with a 90° rotation every 30 min. Coated samples were rinsed twice with PBS before further experimentation.

Plasma immersion ion implantation (PIII) treatment. PIII treatment was applied to electrospun silk samples to achieve surface activation by generating radicals, enabling covalent attachment of rDV.[23] Electrospun silk sheets were mounted onto a metal substrate holder, with a metallic mesh placed 5 cm in front of the sample. The substrate holder was placed into the vacuum chamber and evacuated to a base pressure of 5×10^{-5} Torr. Nitrogen gas was introduced at a flow rate of approximately 72 standard cubic centimeters to generate a pressure of 2×10^{-3} Torr. The source of ions for PIII treatment was generated from inductively coupled radio frequency plasma (13.56 MHz), with a forward power and a reverse power of 100 W and 12 W, respect-

ively. Acceleration of plasma ions was achieved with 20 kV bias pulses of 20 μs duration to the substrate holder and mesh at a frequency of 50 Hz for 800 s. The sample holder was earthed between pulses. Samples were aged for 1 week at room temperature before use to ensure sample homogeneity and to reduce the potential damage to cells caused by free radicals. 6 mm diameter circular disks were prepared using a biopsy punch, and biofunctionalization with rDV on PIII-treated silk disks was conducted as described above for passive adsorption.

PIII treatment of silk tubular scaffolds were performed using a dielectric barrier discharge system[29] specifically developed to enable ion implantation on the internal surfaces of tubular structures[30] and the inner surfaces of porous scaffolds.[29,31] This new process, termed packed-bed plasma ion implantation (PBPII) allows PIII treatment of inner surfaces of tubes without risking damaging the grafts by having to invert and mount them onto an electrically conducting cylinder as was done to achieve PIII treatment of commercially available ePTFE vascular grafts in prior work.[32] Briefly, silk tubular scaffolds were loaded and sealed in a plastic tube with a negative voltage electrode wrapped around the plastic tube at the center and two earth electrodes placed inside the plastic tube 20 cm away from the center on either side. The scaffold assembly was placed into a vacuum chamber and evacuated to a base chamber pressure of 5×10^{-3} Torr, and a base pressure below 0.1 Torr inside the tubular scaffolds. Nitrogen gas was subsequently introduced at a flow rate of 0.1 standard cubic centimeters per minute, resulting in a pressure of ~3 Torr inside the tubular scaffolds. Plasma was ignited inside the tubular scaffolds and accelerated to the internal surfaces by applying a negative high voltage (−8 kV, 500 Hz, 20 μs) for 30 min. Biofunctionalization with rDV on PIII-treated tubular silk scaffolds were conducted within 2 h post-PIII treatment and carried out as described above for passive adsorption.

To confirm immobilization of rDV on electrospun silk scaffolds *via* PIII treatment, rDV was labeled using the Alexa Fluor 594 protein labeling kit (ThermoFisher) according to the manufacturer's instructions and immobilized on silk scaffolds as above. Functionalized scaffold samples with fluorescent rDV were incubated with sodium dodecyl sulphate (SDS, 5% w/v in deionized water, 300 μL) at 60 °C for 1 h and washed 4–5 times with Dulbecco's phosphate buffered saline pH 7.4 (PBS). Samples were transferred into a black 96-well plate, and the fluorescence (590/618 nm) was measured using a plate reader (Multimode plate reader i3X Spectramax, S/N 363703906). The amount of immobilized rDV on silk mats and tubes with or without PIII treatment post-SDS-washing was compared with functionalized scaffolds before SDS washing.

2.5. Characterization of electrospun silk scaffolds

Fiber morphology. Scaffold fiber morphology was visualized using scanning electron microscopy (SEM). Samples were prepared by applying a platinum coating (K575X, Emitech, France) under argon atmosphere for 2 min and imaged using a Hitachi SEM3400I. Fiber diameter was measured using ImageJ.

Mechanical testing. Tensile testing of the electrospun silk scaffolds with or without PIII treatment was performed using Instron model 5543. Samples were prepared as 40 × 5 mm rectangular strips and hydrated in PBS for 30 min. Sample thickness was measured using digital calipers prior to each test. Each strip was clamped into the mechanical testing machine (Instron 5543) with a 20 mm gauge length, and force was measured using a 50 N load cell pulled at an extension rate of 3 mm min^{-1} until fracture. All tests were performed in a 37 °C PBS bath to resemble physiological conditions. Data was collected as load-extension (Bluehill 2 software, version 2.15), converted into stress–strain, and Young's modulus, ultimate tensile strength (UTS), and elongation were calculated. Young's modulus was calculated as the gradient of the linear slope region of the stress–strain curve taken from 1–15% strain.

Swelling test. The swelling behavior of the electrospun silk scaffolds was investigated by incubation of dry samples of known weight in PBS at 37 °C over 10 days. Mass of scaffolds was recorded at 1-, 4-, 7- and 10-days using a 5-digit balance. Before each measurement, sample was removed from PBS and gently tapped on paper towel three times to remove excess PBS. Swelling percentages were then calculated. Silk fibers were also visualized at each time point by staining with rhodamine-phalloidin (1 : 200 dilution, Life Technologies, R415) for 30 min at 37 °C. Samples were rinsed 3 times with PBS and imaged with a confocal microscope (TCS SP2, Leica) using a 40× objective at the center field of view.

2.6. Cell interaction studies on electrospun silk mats

Human umbilical vein endothelial cells (HUVECs) (Lonza, C2519A) and human coronary arterial smooth muscle cells (HCASMCs, Cell Applications Inc.) were maintained in T75 tissue culture flasks with 10 mL of EGM-2 (made up using EGM-2 Bullet Kit (Lonza, CC4176) to the endothelial cell basal medium (EBM-2) (Lonza, CC3156)) or SmGM-2 (made up using SmGM-2 Bullet Kit (Lonza, CC3182) with the smooth muscle cell basal media (SmBM-2) (Lonza, CC3181)), respectively, and incubated at 37 °C with 5% CO$_2$. When 85% confluence was achieved, the cells were rinsed with sterile DPBS followed by treatment with trypsin (3 mL per T75 flask) and incubated at room temperature for 3 min. Once the cells had detached from the flask, EGM-2 or SmGM-2 (7 mL) was added to the flask to neutralise the trypsin. The cell suspension was collected and centrifuged at 1000 rpm for 3 min and the cell pellet was then resuspended in fresh medium. Cells (1 × 10^6) were seeded in a new flask with EGM-2 or SmGM-2 (10 mL). Medium was refreshed every 3–4 days. Cells were used at passages 3–6.

Cell adhesion. HUVECs or HCASMCs (10^4 per well) in EBM-2 basal medium or SmBM basal medium (Lonza) were seeded onto 6 mm electrospun silk disks placed in 96-well plates for 3 h at 37 °C, 5% CO$_2$. Sample conditions included tissue culture plastic (TCP; positive control), blocked TCP (bTCP: denatured 1% w/v BSA in PBS, heated at 90 °C for 10 min and immediately cooled on ice, sterilized using a 0.22 µm syringe filter, coated on TCP scaffolds for 1 h at 37 °C and rinsed twice with PBS; negative control), and electrospun silk with or without PIII treatment in the presence and absence of rDV biofunctionalization. TCP scaffolds were prepared by cutting Thermanox coverslips (ProSciTech) with a 6 mm biopsy punch. After cell seeding and incubation, wells were washed twice with PBS and frozen in a −80 °C freezer. For analysis, the plate was thawed to room temperature before the addition the CYQUANT® GR dye per cell lysis buffer (200 µL, ThermoFisher, C7026). The plate was then incubated for 5 min on the rocker while being protected from light, and then the fluorescence (485/535 nm) was measured using a plate reader (Infinite® 200 PRO, TECAN).

Cell morphology was observed *via* imaging. Briefly, wells were washed twice with PBS, fixed with 4% paraformaldehyde for 15 min at 37 °C, and permeabilized (300 mM sucrose, 50 mM NaCl, 3 mM MgCl$_2$, 2 mM HEPES, 0.5% v/v Triton X-100, pH 7.2) for 5 min at 4 °C. The scaffolds were then blocked in 1% w/v BSA in PBST (0.05% w/v Tween 20 in PBS), for 1 h at room temperature. Samples were rinsed with PBST and stained with rhodamine phalloidin (1 : 200 dilution, Life Technologies, R415) and TO-PRO-3 (1 : 1000 dilution, Life Technologies, 3605) for 30 min in the dark at 37 °C. Cells were rinsed 4 times with PBS and imaged with a confocal microscope (TCS SP2, Leica) using 40× objective at the center field of view. Images were taken as Z-stacks with the same number of image slices and presented as maximum-intensity projections.

Cell proliferation. HUVECs or HCASMCs (10^4 per well) in EGM-2 or SmGM-2 growth media (EBM-2 basal medium with EGM-2 Bullet Kit or SmBM basal medium with SmGM-2 Bullet Kit, Lonza) were seeded onto electrospun silk disks placed in 96 well plates and cultured for 10 days at 37 °C, 5% CO$_2$. Sample conditions included TCP (positive control), bTCP (negative control), rDV-TCP, and 6 mm electrospun silk samples with or without PIII treatment in the presence and absence of rDV biofunctionalization. The following day after cell seeding, samples were washed twice with PBS and transferred to a fresh 96 well plate and cell proliferation was assessed on 1-, 4-, 7- and 10-days post-seeding using the Alamar Blue Cell Viability Reagent.

Cell functionality. 10-Day post-seeding samples were fixed, permeabilized, and blocked with 1% BSA/PBST as described above. Samples were then probed with anti-VE cadherin antibody (50 µL, 1 µg ml^{-1}; Abcam, ab33168) or anti-PCNA antibody (50 µL, 1 µg ml^{-1}; Abcam, ab18197) overnight at 4 °C. Samples were rinsed twice and incubated with corresponding fluorescent secondary antibody (1 : 500; ThermoFisher Scientific) for 30 min at room temperature. Samples were rinsed twice with PBST, stained with rhodamine phalloidin and TO-PRO3 Iodide as described above and imaged with a confocal microscope (TCS SP2, Leica) using 40× objective at the center, center top and center bottom field of view as Z-stacks with the same number of image slices and presented as maximum-intensity projections. VE-cadherin and PCNA staining were quantified using Image J by measuring fluorescence intensity.

2.7. Endothelial cell interaction studies on tubular electrospun silk scaffolds

Medical grade silicone was applied to the outer layer of tubular electrospun silk scaffolds to prevent leakage of the cell culture medium during the 3D cell interaction studies. Silicon casting resin parts A and B were premixed in a 1 : 20 ratio and applied to the outer surface of the silk scaffolds using a fine-tip brush. Silicone coating was cured in a 37 °C incubator for 3 h. Silicone infiltration into the graft lumen was analyzed using Fourier transform *infra*-red spectroscopy (FTIR). The absorbance FTIR spectra of the luminal surface of silk scaffolds, silicone-coated silk scaffolds, and silicone only were recorded with a FTIR spectrometer (Vertex 70V, Bruker). Spectra was recorded from 4000–400 cm^{-1} with the number of scans set to 1000 at a spectral resolution of 4 cm^{-1}.

Endothelial cell adhesion on tubular silk scaffolds. Sample conditions included 6 mm inner diameter ePTFE (control, Teflon®, Gore-tex) with or without rDV, and silk and PIII treated silk with or without rDV. For PIII-treated scaffolds, samples were coated with silicone post-surface treatment. For rDV functionalized samples, rDV was coated on tubular scaffolds as described in Section 2.4 prior to cell seeding. HUVEC cells (2×10^6) in EGM-2 growth medium (500 μL) were injected in 6 mm diameter tubular scaffolds and sealed using a syringe on each end. To account for gravity and ensure uniform cell distribution around the tube's surface, the setup was incubated for 2 h at 37 °C with a 90° rotation every 30 min. Tubular scaffolds were either cut open to form an electrospun silk sheet and fixed and processed for confocal imaging as described above or loaded on the dynamic cell culture setup for the cell retention study in the section below.

Endothelial cell retention on tubular silk scaffolds. To observe endothelial cell retention, cell-seeded scaffolds were loaded on a dynamic cell culture setup in a closed loop consisting of a peristatic pump, a bottle containing EGM-2 growth medium (50 mL), two scaffolds (6 mm in diameter, 2 cm in length) in parallel connected using sterile PVC tubing (2 mm in diameter) and valve fittings. Flow rate was set at 2.5 mL min^{-1} and scaffolds were incubated at 37 °C, 5% CO$_2$ for 2 h. The scaffolds were then fixed and processed for confocal imaging.

2.8. Chick chorioallantoic membrane (CAM) assay with electrospun silk scaffolds

Fertilized Barter black chicken eggs were supplied by Barter and Sons Hatchery, NSW, Australia. All procedures were conducted in accordance with animal ethics protocols approved by the UNSW animal ethics committee (18/16A). All experiments were performed under aseptic conditions. On embryonic development day 0 (E0), eggs were cleaned with 70% ethanol and incubated in a poultry incubator (MultiQuip) at 37 °C, 40–50% humidity with constant rotation. On E4, albumen (4–5 mL) was aspirated from the acute pole of the egg using a 19G needle to create a false air sac directly over the CAM, allowing its dissociation from the eggshell. A circular

window with a 10 mm radius was opened in the eggshell using scissors and sealed with a transparent film dressing (LivingStone) to prevent dehydration and infection. The eggs were returned to the incubator and incubated horizontally with the window facing up and without rotation. On E8, a 9 mm inner diameter silicone ring was placed on top of the CAM and one 3 mm diameter circular silk disks ($n = 6$ per condition) was placed within the silicone ring. Samples included PBS (50 μL per ring) as negative control, VEGF165 (100 ng mL^{-1}, 50 μL per ring) as positive control, and silk disks with or without PIII treatment, in the presence or absence of rDV functionalization. On E13, the CAM was excised around the silicone ring and imaged under a dissecting microscope (LEICA M80, Germany) at 2.5× magnification. The number of blood vessel branches intersecting the scaffold edges and the number of branches in 20 mm^2 area around the sample were counted using ImageJ, as previously described.[19]

2.9. Statistical analyses

All experiments were performed with technical replicates of $n \geq 3$ and at least two independent experiments were performed. Data are presented as mean ± standard deviation (SD) of the technical replicates in one experiment. Statistically significant differences were determined by either a Student's *t*-test one- or two-way analysis of variance (ANOVA) and the Tukey's multiple comparison post-test using GraphPad Prism 9 software. For all analyses, differences were considered significant at $p < 0.05$.

3. Results and discussion

3.1. PIII treatment does not affect the bulk mechanical properties of electrospun silk scaffolds

Electrospun silk scaffolds were manufactured from regenerated silk fibroin solution. Briefly, aqueous silk fibroin was electrospun into tubular scaffolds with the addition of PEO (5% w/v) which increases the viscosity and processability of silk fibroin solution,[33] water annealed to introduce β-sheet crystallization, which allows stability of the scaffolds in aqueous environments with their content influencing degradation rates,[34,35] and soaked in water to remove PEO before PIII treatment.

PIII is known as a surface modification method with low penetration depth (10–100 nm),[24] however, this process has been previously reported to increase surface stiffness.[36,37] Therefore, the effect of the PIII treatment on the surface and bulk mechanical properties of the electrospun silk biomaterials was investigated. The macroscopic changes of the electrospun silk scaffolds were observed *via* photographic images (Fig. 1A). A color change from white to a uniform light brown was noted following the PIII treatment, which is the same as previous reports[24,36] and indicates homogeneous treatment across the surface. This change in color is attributed to the formation of carbonized structures on the surface after energetic ion bombardment of the surface and alteration of the surface functional groups.[36] A similar color change was also observed
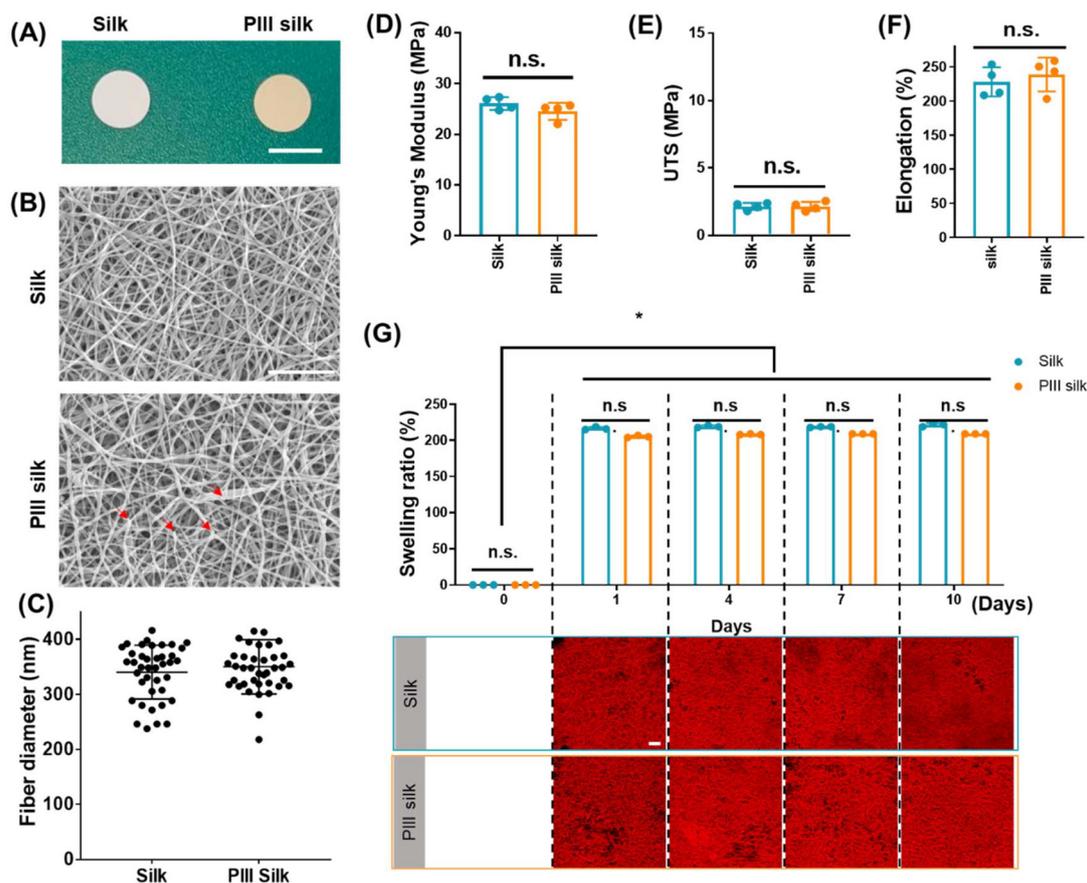
Fig. 1 Morphological and mechanical properties changes of the electrospun silk scaffolds after the PIII treatment. (A) Representative photographic images of electrospun silk scaffolds with or without PIII treatment showing the color change on the scaffold surface following PIII treatment. Scale bar is 5 mm. (B) Representative scanning electron microscope images of the electrospun silk mats with or without PIII treatment. Scale bar is 10 μm. Red arrows point to fiber breakage. (C) Fiber diameter was analyzed from the SEM images using ImageJ, and each datapoint represents one fiber diameter measurement. Electrospun silk mats with or without PIII treatment were cut into 40 × 5 mm strips and hydrated in PBS, submerged in a 37 °C PBS bath and placed under tensile extension using a 50 N load cell until fracture. Quantitative analysis was done by calculating, (D) Young's modulus, (E) ultimate tensile strength (UTS), and (F) elongation-at-break from the stress-strains curves. Data are mean ± SD (n = 4). (G) Electrospun silk samples of known dry weight with or without PIII treatment were soaked in PBS at 37° C over 10 days. Swelling percentages were calculated and fiber morphology was observed at each time point using confocal imaging. Scaffolds were stained with rhodamine phalloidin to show the fibers. Data are mean ± SD (n = 3). * denote significant difference relative to day 0. Scale bar is 50 μm. n.s. indicate no statistically significant difference (p > 0.05) analyzed by Student's t-test.

on silk materials after ultraviolet irradiation as a result of altered tyrosine content.[38]

The scaffold morphology with or without PIII treatment was observed under SEM for the identification of microscopic morphological changes on the silk surface. Electrospinning results in fibrous structures with randomly oriented nano-fibers, as observed in Fig. 1B. Fiber breakage was noted on the surface of the electrospun silk scaffolds after the PIII treatment, likely due to the stress relief within the stiff surface layer generated by the PIII treatment.[39] Similarly, surface cracks were observed on Elast-Eon E2A, a polyurethane block copolymer, following the PIII regimes due to the formation of brittle silicon oxide surface crust generated after ion bombardment.[39] Quantification of the fiber diameter from the SEM images (Fig. 1C) revealed that there was no significant difference between the average fiber diameter of the electrospun silk scaffolds with or without the PIII treat-

ment (341 ± 48 nm vs. 350 ± 49 nm), suggesting that PIII treatment did not affect the fiber diameter. Thus, the PIII treatment on electrospun silk scaffolds induced a color change and some fiber breakage on the treated surface but did not alter the fiber diameter compared to untreated silk.

While PIII treatment is a surface modification method, fiber breakage was observed on the treated surface of the electrospun silk scaffolds. Therefore, it was important to determine whether this treatment impacted the mechanical properties of the bulk material (Fig. 1D–F). Uniaxial tensile testing was performed as an indicator to assess the effects of PIII on the bulk mechanical properties of the material. Silk scaffolds were cut into rectangular strips, submerged in a PBS bath at 37 °C to mimic physiological conditions, and placed under tensile loading until fracture. Young's modulus (Fig. 1D), ultimate tensile strength (UTS) (Fig. 1E) and elongation (Fig. 1F)

were calculated from the stress–strain curves. Electrospun silk scaffolds showed a Young's modulus of 26 ± 1.24 MPa, UTS of 2.14 ± 0.26 MPa, and elongation of 228 ± 21% before breakage. These tensile properties of the electrospun silk scaffolds align with previous reports[40,41] with differences likely attributed to the electrospinning parameters,[15] method to induce β-sheets (methanol *vs.* water vapor annealing)[41] and tensile study conditions (wet *vs.* dry).[42] Further, these tensile properties of the silk scaffolds were more similar to rat aorta than ePTFE when measured under the same conditions,[13] suggesting that these scaffolds demonstrate reduced mechanical mismatch to native tissues than ePTFE. The mechanical properties of the scaffolds after PIII treatment were not significantly different from the untreated silk, indicating that the PIII treatment does not affect the bulk mechanical properties of the electrospun silk scaffold. Previously, the bulk mechanical properties of electrospun scaffolds have been reported to not be affected by PIII treatment when the ratio (2.88×10^{-4}) of the treatment depth (100 nm) to the unmodified bulk (3.47×10^{5} nm) is low.[36]

The swelling behavior of the electrospun silk was studied and compared with PIII treated electrospun silk (Fig. 1G) Previous reports suggested that the PIII treatment may influence the swelling behavior of the biomaterial due to the densification and carbonization of the surface.[36] Silk scaffolds demonstrated significant ($p < 0.05$) water absorption after 24 h of incubation in PBS, however, a longer immersion time in PBS did not affect the sample weight. The water absorption of electrospun silk mats is attributed to the porous structure generated by electrospinning.[43] PIII treatment of electrospun silk did not affect the amount of water absorbed as no significant difference was observed when compared with the untreated silk during the whole incubation period. To observe morphological changes of the silk scaffolds after hydration, the fibrous structures of the scaffolds with or without PIII treatment were observed at various timepoints under confocal microscope after being stained with rhodamine-phalloidin. There were no morphological changes such as pore expansion observed between samples at different time points, suggesting that electrospun silk scaffolds remained stable over time. The PIII treated surface presented a similar fiber morphology to the untreated silk surface. These results suggest that the electrospun silk fibers are stable under physiological conditions and their swelling is not affected by the PIII treatment. This is important as the stability of the biomaterial is essential for cell attachment and function post implantation.[44]

3.2. PIII treatment resulted in stronger immobilization of rDV than passive adsorption on electrospun silk biomaterials

To assess the binding strength of rDV to the silk scaffolds with and without the PIII treatment, stringent SDS washes were applied to the functionalized scaffolds and the level of fluorescently labeled rDV remaining on the silk after the washes was compared. Electrospun silk mats and tubular scaffolds with or without the PIII treatment exhibited a similar level of rDV fluorescence (Fig. 2), indicating these scaffolds supported a similar level of rDV binding which was not affected by the 3D
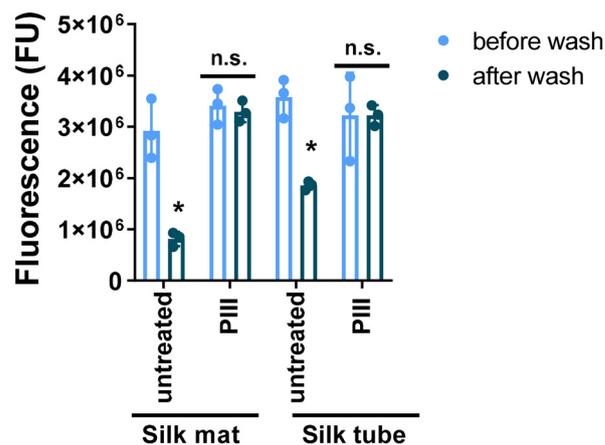

Fig. 2 A stronger immobilization of rDV on electrospun silk was achieved *via* the PIII treatment. The amount of immobilized rDV on silk mats and tubes with or without PIII treatment post SDS-washing was compared with these functionalized scaffolds before SDS-washing. Data are mean ± SD ($n = 3$). * denotes $p < 0.05$ compared to the same condition before wash analyzed by two-way ANOVA.

architecture of the biomaterial. However, a large fraction of rDV was removed from the untreated silk after strong SDS washes compared to that on the PIII treated silk, showing a 72% and 48% reduction on silk mats and silk tubes, respectively. This reduction is attributed the disruption of the electrostatic interactions of molecules on a material surface caused by the anionic SDS.[45] This result suggests a much stronger binding of rDV on electrospun silk scaffolds was achieved *via* the PIII surface treatment. This SDS-resistant binding suggests covalent immobilization of rDV on the PIII activated electrospun silk surface as reported for the immobilization of a variety of biomolecules on biomaterial surfaces.[46–48] A similar result was demonstrated previously on rDV functionalized silk films *via* PIII.[36] This strong rDV binding to the scaffold is important for vascular graft applications as the weakly bound rDV under the shear stress from the blood flow and exposure to the dynamic blood plasma proteins may result in protein displacement by other proteins with stronger binding affinities (the 'Vroman effect') and could lead to unintended biological responses such as thrombosis and graft failure.[49]

3.3. PIII treatment and rDV biofunctionalization modulate vascular cell interactions in 2D cell cultures

While strong rDV immobilization on electrospun silk scaffolds was achieved *via* the PIII treatment, the functionality of rDV after immobilization has not been established. This is particularly important as the function of bioactive molecules is affected by the conformation and orientation on the surface that are governed by the immobilization technique.[18,39,50] Therefore, to investigate the functionality of rDV and the potential of rDV functionalized electrospun silk grafts toward vascular graft applications, interactions of endothelial and smooth muscle cells with the functionalized silk mats were studied in 2D cell culture.

Graft endothelialization is key to maintaining long-term graft patency[51–53] and this process involves adhesion, migration, and proliferation of endothelial cells on the graft.[54] rDV surface biofunctionalization and PIII surface treatment have been previously demonstrated to enhance endothelial cell interactions individually.[18,24,55] Thus, endothelial cell adhesion and proliferation were studied on electrospun silk mats biofunctionalized with rDV via either passive adsorption or PIII treatment and were compared to unfunctionalized silk. rDV concentration on electrospun silk was optimized prior to commencing cell studies (Fig. S2†). HUVECs were then seeded onto untreated electrospun silk mats, or PIII-treated electrospun silk mats in the presence or absence of rDV for 3 h in serum-free medium, and the level of cell adhesion was compared to TCP (positive control), rDV-coated TCP (positive control), and dBSA-coated TCP (negative control). Cell morphology was observed by staining polymerized actin fibers (rhodamine phalloidin, red) (Fig. 3A). HUVECs adhered to positive controls and exhibited a well-spread morphology with polymerized actin fibers, while cells did not adhere to the negative control. Few HUVECs adhered on silk without rDV, and these cells appeared small and round. Biofunctionalization of electrospun silk with rDV via passive adsorption supported more cell adhesion, and cells were larger in size. However, these cells were less spread when compared to the positive controls. PIII-treated silk also supported more cell adhesion than untreated silk, but cells were not well-spread compared to the positive controls. Biofunctionalization of PIII-treated electrospun silk with rDV did not appear to have any effect on cell adhesion or cell morphology relative to the unfunctionalized PIII-treated silk. HUVEC adhesion to the different silk surfaces was quantified by the CyQuant Cell Proliferation Assay (Fig. 3B). Quantifying the HUVEC cell adhesion supported qualitative observations that the unmodified silk supported little HUVEC cell adhesion comparable to the negative control. Biofunctionalization of silk with rDV via passive adsorption significantly ($p < 0.05$) enhanced HUVEC adhesion, exhibiting a 2.4-fold increase relative to silk alone. Cell adhesion on PIII treated silk was significantly ($p < 0.05$) higher than silk, with a 3.5-fold higher cell adhesion detected on PIII treated silk when compared to silk alone. Biofunctionalization of PIII-treated silk with rDV showed a comparable level of cell adhesion to the unfunctionalized PIII-treated silk. HUVEC spreading was quantified by measuring the cell area (Fig. 3C), which confirmed qualitative observations that TCP supported the highest level of cell spreading while cells on rDV-coated TCP showed a 2.7-fold lower cell spread area. Silk mats supported little cell spreading, exhibiting an 8-fold lower cell spreading relative to TCP control. Neither rDV biofunctionalization nor PIII treatment enhanced cell spreading compared to untreated silk.

Collectively, unmodified electrospun silk did not support endothelial cell adhesion, which was expected as silk possesses no inherent cell binding domains,[18] and supports weak cell interactions.[56] This result is similar to previous reports where human coronary artery endothelial cell (HCAEC) adhesion to unmodified silk films was low.[18] Biofunctionalization of electrospun silk with rDV via passive adsorption supported more endothelial cell adhesion compared to unfunctionalized silk. This is consistent with previous
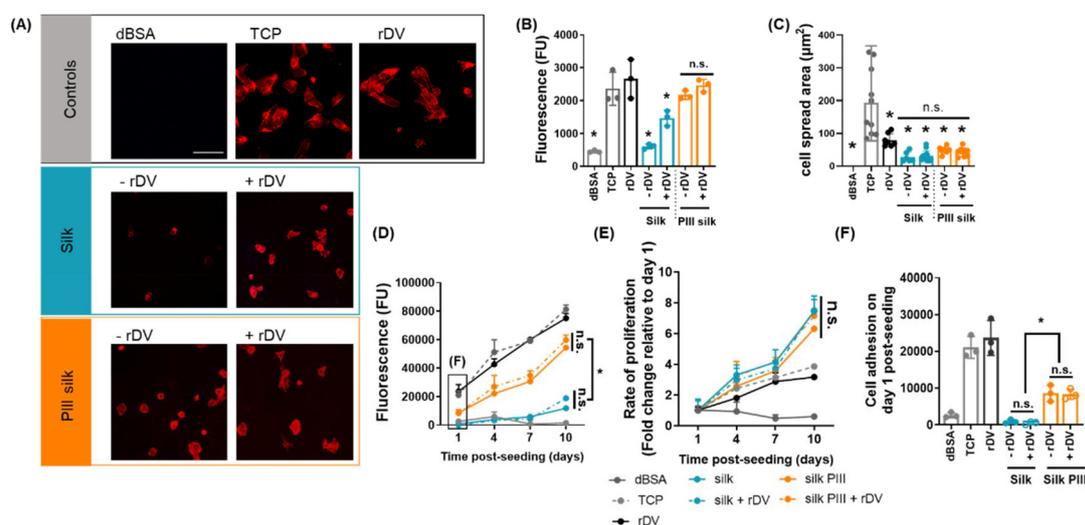
Fig. 3 PIII treatment promotes HUVEC adhesion and proliferation on electrospun silk mats. (A) HUVEC morphology at 3 h post-seeding on silk mats biofunctionalized with rDV via passive adsorption or PIII treatment and compared to negative control (denatured BSA (dBSA–coated TCP), and positive controls (TCP) and rDV-coated TCP (rDV)). Cells were stained to show polymerized actin fibers (rhodamine phalloidin, red). Scale bar is 100 μm. Cell adhesion on silk mats was quantified using the CYQUANT assay (B), and cell spreading was quantified by measuring the cell area using ImageJ (C) compared to TCP control (mean ± standard deviation, $n = 3$). (D) Cell proliferation was studied using Alamar blue cell metabolic assay on days 1, 4, 7, and 10 post-seeding and data from day 1 post seeding is plotted separately as (F). (E) The rate of cell proliferation was calculated relative to the fluorescence at day 1 for each condition. Data are presented as mean ± standard deviation ($n = 4$). * denotes $p < 0.05$ analyzed by two-way ANOVA.

reports where electrospun silk with passively adsorbed rDV supported HCAEC adhesion.[21] rDV support for endothelial cell adhesion is attributed to the cell interaction with the $\alpha_2\beta_1$ integrin binding site within the LG3 region of rDV.[55] PIII surface-modified electrospun silk demonstrated more endothelial cell adhesion relative to the unmodified silk, which aligns with previous research that PIII-treated silk films enhanced bovine arterial endothelial cell (BAEC) adhesion to the surface.[24] Interestingly, the biofunctionalization of PIII-treated silk with rDV did not further enhance endothelial cell adhesion relative to the unfunctionalized PIII-treated silk. One possible explanation is that the PIII treatment of silk resulted in maximum endothelial cell adhesion on silk under these current experimental conditions and the effect of rDV on endothelial cell interaction was masked.

To investigate the effect of electrospun silk mats on the proliferation of endothelial cells, HUVECs were seeded onto untreated or PIII-treated electrospun silk mays in the presence or absence of rDV for 10 days in a serum-containing medium, and the level of cell proliferation was measured with the Alamar Blue assay over the analysis period (Fig. 3D) and the proliferation rate was calculated relative to the fluorescence detected at day 1 for each condition (Fig. 3E). Electrospun silk mats and the positive controls supported endothelial cell proliferation over the 10-day culture period where cells exhibited exponential cell growth ($R^2 > 0.95$) as indicated by the increasing cell metabolic activity over time. Relative cell number on electrospun silk with or without the passively adsorbed rDV was low, while the PIII-treated silk with or without the rDV biofunctionalization supported significantly ($p < 0.05$) higher number of cells compared to silk at all time points (Fig. 3D), indicating that PIII treatment enhanced endothelial cell proliferation on silk mats. Interestingly, the biofunctionalization of silk or PIII silk with rDV did not result in a significant difference in endothelial cell proliferation when compared to their unfunctionalized counterparts. While obvious differences in endothelial cell proliferation were observed between different electrospun silk preparations, the rates of endothelial cell proliferation on different electrospun silk mats were similar (Fig. 3E). In contrast, cell adhesion on day 1 post-seeding showed that significantly more cells adhered to the PIII-treated silk mats than the untreated silk, while the rDV biofunctionalization did not show any effect (Fig. 3F). This trend matched the endothelial cell proliferation presented in Fig. 3D, suggesting that the cell adhesion on day 1 post-seeding is the major contributor to the observed cell proliferation differences. Interestingly, the cell adhesion 3 h post-cell seeding was significantly improved by the rDV biofunctionalization on electrospun silk, as presented in Fig. 3B. We hypothesize that the observed discrepancy is primarily due to the presence or absence of serum in the endothelial cell cultures. In Fig. 3B, the cell adhesion assay was conducted in serum-free media to evaluate the direct effect of rDV on endothelial cell adhesion. Under these conditions, rDV effectively promoted cell attachment. However, in Fig. 3F, the 24 hour adhesion assessment was performed in serum-containing

media, as this experiment was part of the cell proliferation study. In the presence of serum proteins and over a longer culture period, passively adsorbed rDV may have been displaced due to competitive protein exchange (the Vroman effect), leading to the observed reduction in adhesion enhancement. Interestingly, this trend was not observed for PIII-treated samples, suggesting that covalent immobilization *via* PIII provides a more stable interface that supports both early and sustained endothelial cell attachment. Collectively, PIII surface modification and the rDV biofunctionalization were shown to support endothelial cell proliferation on the silk biomaterial, but did not affect the cell proliferation rates. This is consistent with previous studies demonstrating that the PIII treatment and rDV biofunctionalization can enhance BAEC[24] and HUVEC[57] proliferation.

While PIII treated silk with or without rDV biofunctionalization demonstrated enhanced endothelial cell adhesion and proliferation, it is important to determine the functionality of the endothelial layer on electrospun silk mats. Vascular endothelial (VE)-cadherin is an endothelial-specific cell–cell adhesion protein that plays a key role in maintaining the endothelial barrier function[58,59] and cells modulate their cell–cell adhesion state by controlling the amount of VE-cadherin at the cell surface.[58] Thus, VE-cadherin expression was studied to assess the functionality of the endothelial layer on the electrospun silk mats. Scaffold samples were collected at the endpoint of the proliferation assay after the 10-day culture period; cells were fixed and stained for VE-Cadherin and F-actin. Representative images of each stain and merged images are shown in Fig. 4A. Overall, HUVECs formed a confluent cell layer on PIII-treated electrospun silk mats in the presence or absence of rDV, but not on the untreated electrospun silk in the presence or absence of rDV. This is consistent with the endothelial cell proliferation result presented in Fig. 3D. Electrospun silk samples with or without passively adsorbed rDV did not support VE-cadherin expression as the VE-cadherin was localized within the cells for both conditions. This is likely attributed to the low cell number on the scaffolds and the large gaps between cells. PIII treatment enhanced the expression of VE-cadherin on electrospun silk mats where VE-cadherin was localized to the cell periphery and cell–cell junctions. This high level of VE-cadherin expression is critical for a functional graft endothelium that can contribute to maintaining a stringent blood-graft barrier.[60] Interestingly, multi-cellular structures were formed on these PIII-treated silk mats with or without rDV biofunctionalization which is key to the formation of primitive blood vessels.[61] The effect of rDV was evident on rDV functionalized TCP and PIII-treated silk when compared with the unfunctionalized counterparts that the VE-cadherin staining was more defined around the cell boundaries and less diffused within the cells. This result indicates that rDV enhanced the integrity of cell–cell contacts on PIII-treated electrospun silk and confirmed the bioactivity of rDV immobilized on electrospun silk mats *via* PIII treatment.

VE-cadherin was quantified by measuring the fluorescence intensity of the VE-cadherin staining (green channel) (Fig. 4B)
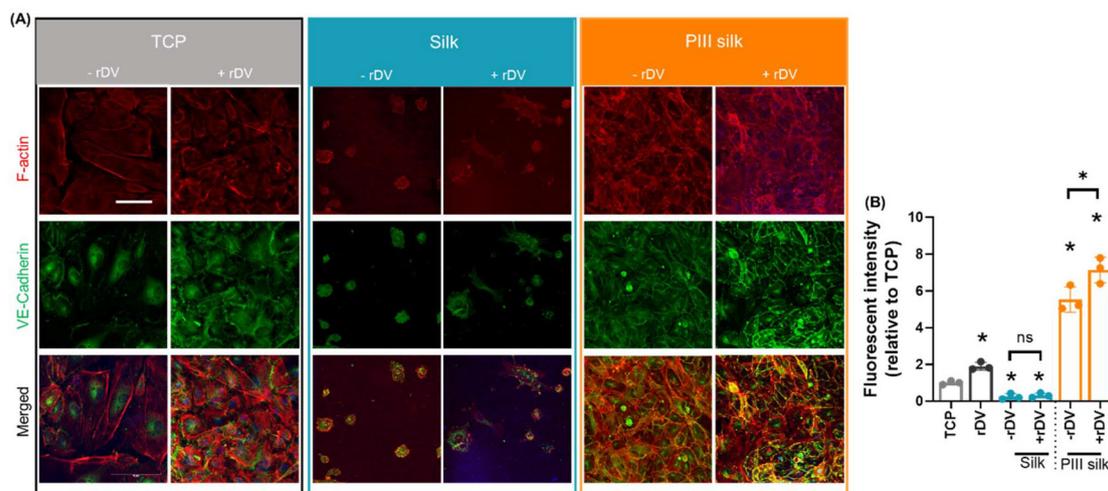
Fig. 4 rDV and PIII treatment enhanced HUVEC cell–cell interactions on electrospun silk mats. HUVECs were seeded onto silk or PIII-treated silk biomaterial with or without rDV, negative control (dBSA-coated TCP), or positive controls (TCP and rDV-coated TCP) and cultured for 10 days. (A) Cells were then fixed and stained for VE-Cadherin (green) and F-actin (red). Scale bar is 20 μm. Images were taken as z-stacks with the same number of image slices and presented as maximum intensity projections. (B) The fluorescence intensity of the VE-cadherin was measured for each condition ($n = 3$). Images were taken using the same laser power and gain, same depth of z-stacks were imaged with the same number of image slices. Unless indicated otherwise, * denotes $p < 0.05$ compared to TCP analyzed by one-way ANOVA.

and aligned with the qualitative observations that rDV enhanced VE-cadherin expression by 1.9-fold relative to coated TCP. Cells plated on silk biomaterials exhibited significantly ($p < 0.05$) lower levels of VE-cadherin expression compared to cells on TCP, while the presence of rDV did not enhance VE-cadherin expression. In contrast, cells on PIII-treated silk displayed a significantly ($p < 0.05$) increased VE-cadherin expression (5.5-fold increase relative to the TCP control), and the rDV biofunctionalization on PIII-treated silk further enhanced the VE-cadherin expression by 1.3-fold compared to the unfunctionalized PIII-silk counterpart.

Stenosis is a major cause of late-stage graft failure primarily due to neointimal hyperplasia at the anastomoses,[62] which is caused by the over-proliferation of smooth muscle cells into the tunica intima.[63] Thus, biomaterials that can promote endothelialization while inhibiting smooth muscle cell proliferation are desired for vascular graft applications. rDV has been previously shown to inhibit smooth muscle cell adhesion,[55,64] hence the interactions between rDV biofunctionalized silk mats and vascular smooth muscle cells were studied, including cell adhesion, proliferation, and the cell phenotype.

Similar to HUVECs, HCASMCs were seeded onto untreated, or PIII-treated electrospun silk mats in the presence or absence of rDV for 3 h in serum-free medium, and the level of cell adhesion was compared to TCP (positive control), rDV coated TCP (negative control, as rDV does not support SMC interactions), and dBSA-coated TCP (negative control). Cell morphology was observed by staining polymerized actin fibers (rhodamine phalloidin, red) (Fig. 5A). HCASMCs adhered to the TCP positive control exhibited a well-spread morphology with polymerized actin fibers, while cells exhibited a round

morphology with actin present at the radial protrusions on rDV-coated TCP. This is similar to previous reports which demonstrated that rDV inhibits smooth muscle cell adhesion.[22] HCASMCs adhered on electrospun silk in the absence of rDV, and these cells appeared in a similar morphology to the cells on TCP, but with a reduced number of cells. Biofunctionalization of electrospun silk with rDV via passive adsorption reduced cell adhesion and cells appeared more rounded and less spread. PIII-treated silk supported more cell adhesion relative to the untreated silk, and cell morphology was similar to the positive control. Biofunctionalization of PIII-treated electrospun silk with rDV reduced the number of cells adhered, and cell morphology appeared as a mix of well-spread and rounded cells. Cells had a rounded morphology as a result of the rDV coating, which reduces HCASMC adhesion[64] while the well-spread cell morphology is likely the result of the surface chemistry changes from the PIII treatment, which promotes cell interactions.[24] HCASMC adhesion to the different silk surfaces was quantified by the CyQuant Cell Proliferation Assay (Fig. 5B). Quantification of the HCASMC cell adhesion confirmed qualitative observations that the unmodified silk supported little HCASMC cell adhesion that was comparable to the negative control. Immobilization of rDV on TCP, electrospun silk and PIII treated electrospun silk mats all significantly ($p < 0.05$) reduced HCASMC adhesion, exhibiting a 1.8-, 1.4- and 1.6-fold decrease relative to their unfunctionalized counterpart, respectively. This result suggests that the bioactivity of rDV was retained on electrospun silk regardless of the functionalization method. Interestingly, PIII-treated electrospun silk exhibited a significant ($p < 0.05$) 1.4-fold increase in cell adhesion compared to the untreated silk, suggesting PIII treatment
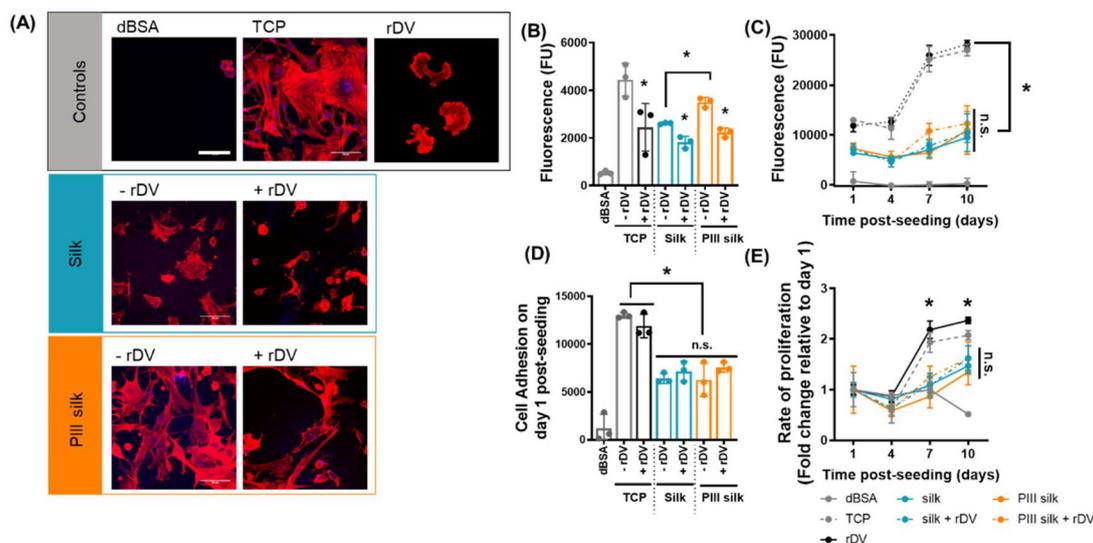
Fig. 5 rDV inhibits HCASMC adhesion on electrospun silk mats. (A) HCASMC morphology at 3h post-seeding on rDV biofunctionalized silk mats *via* passive adsorption or PIII treatment and compared to negative controls (dBSA-coated TCP) and positive controls (TCP and rDV-coated TCP). Cells were stained to show polymerized actin fibers (rhodamine phalloidin, red). Scale bar is 20 μm. Cell adhesion on silk mats was quantified using the CYQUANT assay (B) (mean ± standard deviation, $n = 3$). (C) Cell proliferation was studied by measuring relative cell number (fluorescence intensity) using the Alamar blue cell metabolic assay on days 1, 4, 7, and 10 post-seeding. (D) Cell adhesion on day 1 post cell seeding measured by Alamar blue. (E) The rate of cell proliferation was calculated relative to the fluorescence at day 1 for each condition. Data are presented as mean ± standard deviation ($n = 4$). Unless stated otherwise, * denotes $p < 0.05$ compared to the unfunctionalized counterparts of the scaffolds analyzed by one-way ANOVA.

enhanced smooth muscle cell adhesion. Together with the endothelial cell adhesion data presented in Fig. 3, this shows that the PIII treatment promotes vascular cell interactions non-selectively, which is in agreement with previous reports.[24] Hence, the rDV biofunctionalization is vital as it provides vascular cell selectivity.[18,55]

The effect of electrospun silk mats on the proliferation of vascular smooth muscle cells was investigated by seeding HCASMCs onto untreated or PIII-treated electrospun silk mats in the presence or absence of rDV for 10 days in serum-containing medium. The relative cell number was measured with the Alamar Blue assay over the analysis period (Fig. 5C), and the rate of proliferation was calculated relative to the fluorescence detected at day 1 for each condition (Fig. 5E). Cell metabolic activity on electrospun silk mats was significantly ($p < 0.05$) lower than on TCP at all time points regardless of the surface treatment and biofunctionalization. These differences in smooth muscle cell metabolic activity observed between electrospun silk samples and TCP samples appeared to be related to the rate of proliferation (Fig. 5E) as well as the cell adhesion on day 1 post-seeding (Fig. 5D). The smooth muscle cells on electrospun silk mats exhibited a significantly ($p < 0.05$) slower proliferation rate when compared to the positive control from day 7, while no significant differences were observed between electrospun silk samples with or without the surface modification or rDV biofunctionalization. Similarly, cell adhesion on day 1 post-seeding followed the same trend where significantly ($p < 0.05$) more cells adhered to the TCP samples than electrospun silk, and the surface modification

and biofunctionalization on electrospun silk did not affect the cell adhesion on day 1 post-seeding. This difference in smooth muscle cell proliferation profile on TCP and electrospun silk may be attributed to the difference in smooth muscle cell phenotype,[65] thus, the phenotypes of smooth muscle cells on the various electrospun silk mats and TCP was studied next.

Vascular smooth muscle cells possess phenotype plasticity to switch between proliferative, synthetic and quiescent, contractile phenotypes depending on environmental cues.[65,66] It was hypothesized that the low smooth muscle cell proliferation profile on the electrospun silk mats was a result of the phenotype switching. Thus, vascular smooth muscle cell phenotype was studied on the electrospun silk mats and compared to TCP. Scaffolds were collected at the end point of the proliferation assay and cells were stained for proliferating cell nuclear antigen (PCNA) and nuclei (Fig. 6). After 10 days of cell culture, HCASMCs proliferated on all TCP and electrospun silk surfaces as indicated by the large number of (TO-PRO-3 staining in blue). Many cells on TCP were identified as proliferative but little to no PNCA staining was observed for cells on electrospun silk samples. These results suggested that all cells on TCP were proliferative as indicated by the colocalization of the two stains, while few cells on the electrospun silk samples were proliferative. These results suggested that the HCASMCs initially proliferated on electrospun silk biomaterials and switched to a quiescent state between day 4 and 7 post-cell seeding as a significantly reduced rate of cell proliferation was observed between these two time points (Fig. 5E). This is likely a silk -guided process as all electrospun silk scaffolds, irrespec-
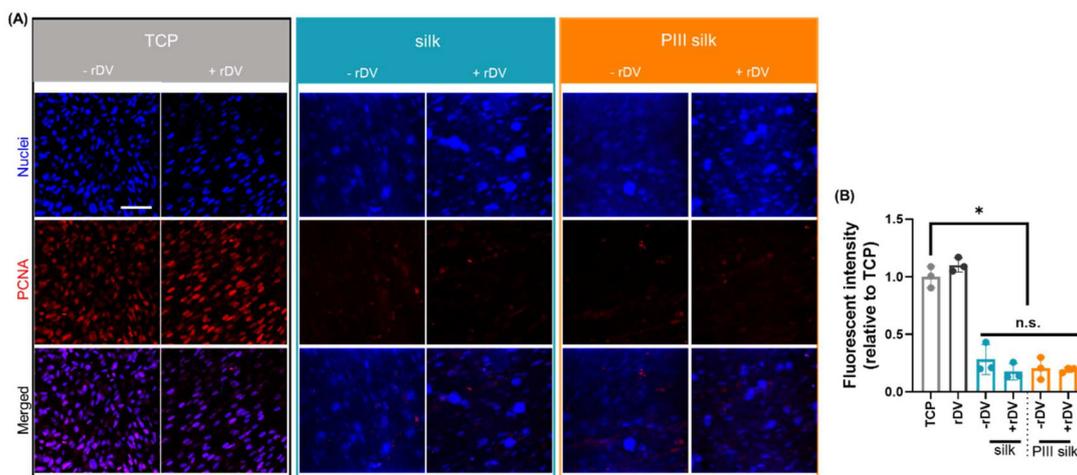
Fig. 6 HCASMCs were maintained in a quiescent state on electrospun silk. HCASMCs were seeded onto silk or PIII-treated electrospun silk with or without rDV, positive control (TCP with or without rDV), and cultured for 10 days. (A) Representative images of cells stained for PCNA (red) and cell nuclei (blue). Scale bar is 20 μm. (B) Fluorescence intensity of the PCNA staining was measured for each condition ($n = 3$). Images were taken using the same laser power and gain, the same depth of z-stacks were imaged with the same number of image slices. Unless indicated otherwise, * denotes $p < 0.05$ compared to TCP control analyzed by one-way ANOVA.

tive of the rDV biofunctionalization or PIII treatment, exhibited the same trend. This is in line with previous research where the smooth muscle cell phenotype switches from synthetic to contractile on electrospun silk vascular grafts *in vivo*.[14] There are many factors that contribute to the phenotype switching,[67] and how silk fibroin contributes phenotype switching in HCASMCs remains to be fully understood.

Collectively, the PIII surface treatment enhanced the ability of electrospun silk mats to support endothelial cell adhesion and proliferation. However, this surface modification technique non-selectively enhances cell interaction as it supports both endothelial and smooth muscle cell interactions. Multiple factors could be contributing to the enhanced cell interaction following PIII treatment, including changes in surface chemistry, wettability, topography, and stiffness of the silk biomaterials.[24] However, it is difficult to isolate individual contributions, and it is likely that all these factors collectively contribute to the observed effects. Thus, the biofunctionalization of electrospun silk mats with rDV is critical as it presents selectivity for different vascular cell types, promoting endothelial cell interactions while reducing smooth muscle cell adhesion on electrospun silk. This selective interaction suggests that the bioactive properties of rDV remain functional and are not masked by the surface modifications induced by PIII. Thus, the combined effect of PIII treatment and rDV on electrospun silk mats holds promise for vascular graft applications.

### 3.4. PIII treatment and rDV modulate endothelial cell interactions in 3D cell cultures

PIII treatment on electrospun silk mats demonstrated enhanced endothelial cell interactions *in vitro* in 2D cell cultures in the previous section, but it is also important to study cell interactions under 3D and dynamic culture conditions, which can better simulate the relevant physiological environment *in vivo* and are more realistic for translating the study findings for *in vivo* vascular graft applications.[68–71]

Electrospun silk grafts (6 mm diameter) were used for the dynamic cell culture studies; however, due to the highly porous structures produced by the electrospinning technique, a medical grade silicone layer was cast onto the outer layer of the electrospun silk grafts to prevent media leakage (Fig. S1A†). The luminal surface was characterized by FTIR (Fig. S1B†) and small changes in the absorbance spectra located at 2950 cm⁻¹ and 800 cm⁻¹ were observed on the silicone coated silk tubes compared to uncoated, and those changes correspond to peaks identified in the absorbance spectra of silicone. This result suggests silicone infiltration to the luminal side, which may affect cell interactions. Therefore, endothelial cell adhesion and proliferation on the silicone coated silk tubes was investigated (Fig. S1C–E†). The lumen of the silicone-coated silk tube exhibited a comparable level of HUVEC adhesion (Fig. S1C†) and proliferation (Fig. S1D and E†) to that of the uncoated silk, suggesting that the ability of silk to support HUVEC interactions were not affected by the infiltrated silicone, thus, the silicone coated electrospun silk grafts were deemed suitable for subsequent 3D cell culture studies.

Endothelial cell adhesion under static conditions was studied by seeding HUVECs on untreated, or PIII-treated electrospun silk tubes in the presence or absence of rDV for 2 h in serum-free medium with a 90° rotation every 30 min (Fig. 7A). The level of cell adhesion was compared to commercial ePTFE grafts and rDV-coated ePTFE grafts by observing cell morphology (Fig. 7B) and quantifying relative cell number by measuring fluorescence intensity of the F-actin staining after
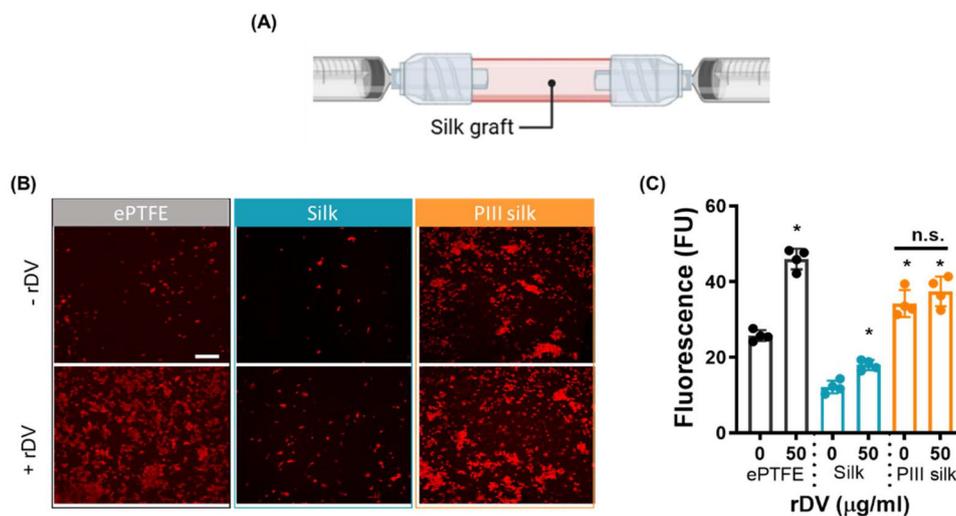
Fig. 7 PIII treatment promotes HUVEC adhesion on tubular electrospun silk. (A) Setup of the static 3D cell culture on tubular scaffolds. Silicone coated silk grafts or ePTFE grafts were attached to 6 mm outer diameter valve fittings and double sealed with Parafilm and zip lock ties to prevent leakage. Zip lock ties also served as position holders to enable 90° rotation of the apparatus. (B) HUVECs were seeded on ePTFE vascular graft with or without rDV, and on rDV biofunctionalized tubular silk tubes *via* passive adsorption or PIII treatment for 2 h. Cells were stained to show polymerized actin fibers (rhodamine phalloidin, red). Scale bar is 50 μm. (C) Cell adhesion was quantified by measuring the fluorescence intensity of the F-actin staining (mean ± standard deviation, $n = 3$). Unless indicated otherwise, * denotes $p < 0.05$ compared to ePTFE or standalone silk analyzed by one-way ANOVA.

the Cyquant assay (Fig. 7C). ePTFE supported a low level of HUVEC adhesion, which is in agreement with previous reports.[72,73] The rDV coating on ePTFE significantly enhanced cell adhesion ($p < 0.05$), exhibiting a 1.8-fold increase in fluorescence intensity. This result suggested the ability of rDV to enhance endothelial cell adhesion is translatable to ePTFE biomaterials. Electrospun silk grafts supported little HUVEC adhesion; however, biofunctionalization with rDV *via* passive adsorption enhanced cell adhesion 1.5-fold. PIII-treated silk also supported more cell adhesion than untreated silk, showing a 2.8-fold increase in the number of adhered cells. However, the biofunctionalization of PIII-treated silk with rDV did not affect cell adhesion relative to the unfunctionalized PIII-treated silk. These results are in agreement with the endothelial cell adhesion on electrospun silk mats in 2D cell cultures shown in Fig. 3B, suggesting that the endothelial cell adhesion properties of rDV biofunctionalization and PIII surface treatment on electrospun silk were transferable from 2D to 3D cell culture.

Endothelial cell retention under shear stress is critical for graft endothelialization *in vivo*;[73,74] thus, the effect of PIII surface treatment and rDV biofunctionalization on the retention of endothelial cells on the ePTFE and electrospun silk was evaluated. Cell-seeded grafts generated from the previous section (Fig. 7C) were placed under flow, as illustrated in Fig. 8A. The dynamic cell culture system consisted of a peristaltic pump, a medium reservoir, and two 6 mm diameter grafts connected by sterile PVC tubing. The two grafts were connected in parallel *via* a three-way valve fitting. After 3 h of dynamic flow at 2.5 mL min⁻¹, the rDV-coated ePTFE grafts exhibited a 1.8-fold increase in the number of cells adhered compared to the uncoated

ePTFE (Fig. 8B and C). This result suggested that rDV not only supported endothelial cell adhesion on ePTFE, but that the adhered cells remained attached under shear stress. Cell retention on electrospun silk in the absence of rDV was low, with only a few cells observed following the dynamic cell culture. Biofunctionalization with rDV *via* passive adsorption did not enhance cell retention with the number of adhered HUVECs comparable with the unfunctionalized silk. This is likely due to the weakly bound rDV *via* passive adsorption being washed off under sheer stress. PIII surface treatment enhanced cell retention on electrospun silk exhibiting 2.3-fold more adhered cells relative to the untreated silk grafts. Biofunctionalization of the PIII-treated silk grafts with rDV further enhanced cell retention, supporting 3- and 1.3-fold more cells relative to the untreated silk grafts and PIII silk without rDV, respectively. These results suggested that rDV immobilized *via* PIII on electrospun silk biomaterials was superior in retaining endothelial cells under dynamic culture conditions, promoting the formation of stable endothelium. Endothelial cell proliferation under flow is an essential step for graft endothelialization and tissue remodeling[75] while mechanical cues generated by the blood flow *in vivo* are a critical contributor to the function of endothelial cells.[76] Thus, endothelial cell proliferation on electrospun silk grafts under flow was observed after a 3-day culture. There was evidence of cell proliferation on electrospun silk tubes around the distal regions, as shown in Fig. 8D. These data suggested that co-valently immobilized rDV on electrospun silk *via* PIII treatment presented the highest level of endothelial cell adhesion and retention underflow in 3D cell cultures, making it worthy of further investigation as a biomaterial to support graft endothelialization *in vivo*.
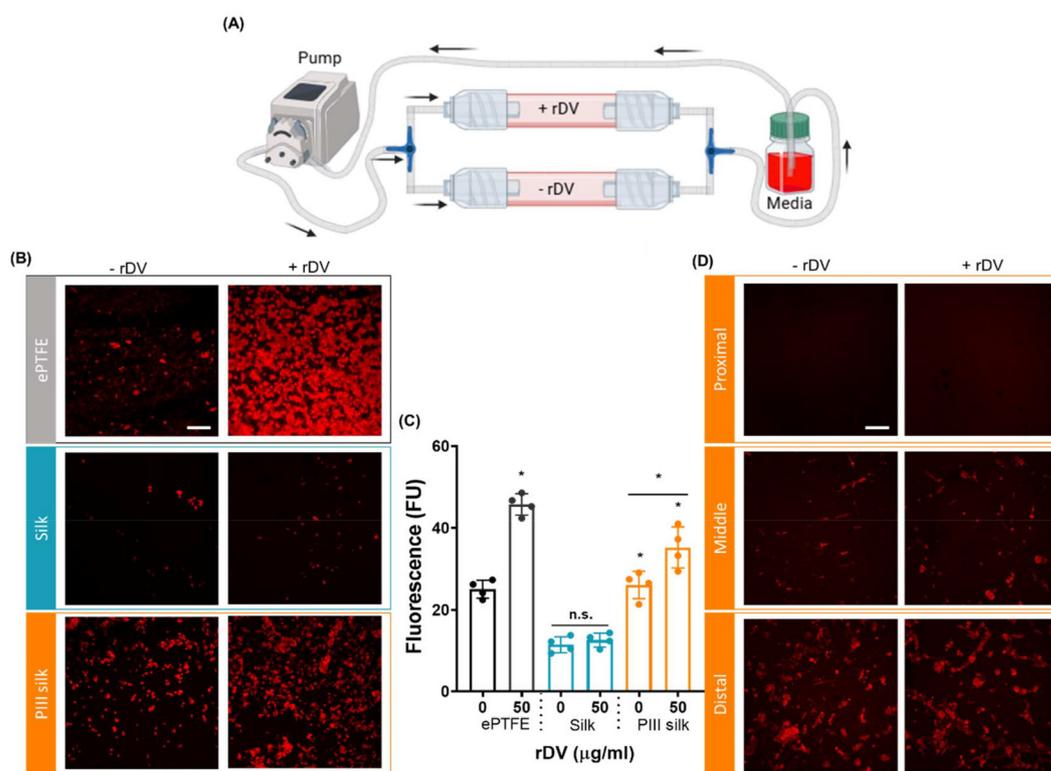
Fig. 8 rDV enhances HUVEC retention on PIII treated tubular electrospun silk biomaterials. (A) Dynamic cell culture schematic diagram. Two tubular scaffolds were connected in a closed loop with the peristatic pump and a medium containing bottle using sterile PVC tubing. Cell seeded grafts from Fig. 7C were loaded onto the dynamic cell culture setup as shown in (A) and cell medium was flowed through the grafts for 3 h. (B) Cells were stained to show polymerized actin fibers (Rhodamine phalloidin, red). Scale bar is 50 μm. (C) Cell adhesion was quantified by measuring the fluorescent intensities of the F-actin staining (mean $\pm$ standard deviation, n = 3). Unless indicated otherwise, * denotes $p < 0.05$ compared to ePTFE or untreated silk grafts analyzed by one-way ANOVA. (D) HUVECs were seeded on PIII-treated tubular silk grafts with or without rDV and loaded onto the dynamic cell culture. Cell medium was flowed through the grafts for 3 days, and cells were stained to show polymerized actin fibers (rhodamine phalloidin, red). Proximal, middle, and distal sections of the graft were imaged. Scale bar is 50 μm.

3.5. PIII surface treatment on electrospun silk enhanced angiogenesis *in vivo*

Three key mechanisms of graft endothelialization have been identified for vascular grafts, including transanastomotic migration, transmural infiltration, and fallout healing from the blood.[54,77] Among these three processes, transmural capillary ingrowth is essential for a confluent vascular graft endothelium formation[77] as these capillaries act as an endothelial cell source to the mid regions of the graft lumen.[78] Vascular grafts that can stimulate endogenous angiogenic responses are likely to induce capillary growth into the graft and lead to graft endothelialization.[79] rDV was demonstrated to promote angiogenesis *in vivo* in the CAM model,[19] therefore, it is of interest to evaluate the angiogenic properties of rDV when immobilized on electrospun silk mats. The CAM assay, as an early-stage screening technique of angiogenic potential, provides a highly vascularized environment that allows direct examination of how biofunctionalized electrospun silk scaffolds influence neovascularization and provides direct insight into how the tubular electrospun scaffolds may contribute to endothelialization and vessel integration *in vivo*. In this section, elec-

trospun silk mats biofunctionalized with rDV *via* passive adsorption or PIII treatment were placed on the CAM to test their angiogenic properties (Fig. 9A and B).

PBS and VEGF165 (100 ng mL^{-1}) were used as negative and positive controls, respectively. However, these samples did not contain a scaffold, so for consistency, a semi-circle the size of half of the scaffold was drawn on the images for these controls. The number of blood vessels intersecting the semi-circle and the number of blood vessels in the highlighted region were then counted (Fig. S3†). VEGF165 (positive control) promoted a significant ($p < 0.05$) 1.5-fold higher blood vessel density relative to PBS (negative control), however, the number of blood vessels intersecting the semi-circle was at a comparable level with the PBS (Fig. 9B and C). This result suggested the angiogenic effect of VEGF165 supported an even increase in the number of blood vessels in the area which was exposed to the growth factor and this effect was not obvious in a small region. Electrospun silk mats did not enhance blood vessel formation relative to PBS. This result is in contrast with a previous report which showed silk fibroin scaffolds induced angiogenesis.[80] This difference is likely attributed to the different scaffold fabrication methods and scaffold incubation
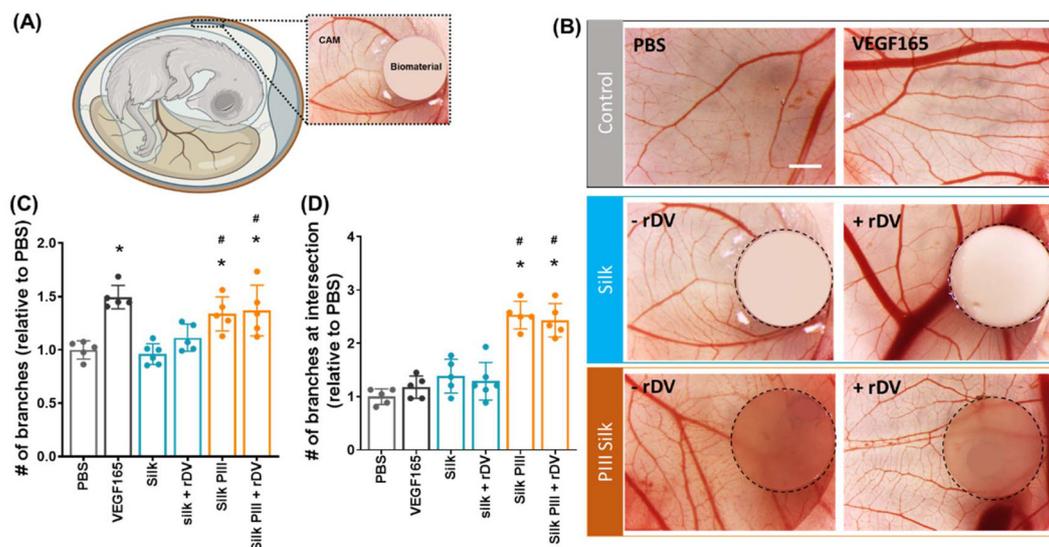
Fig. 9 PIII treated silk mats promoted angiogenesis *in vivo* in the CAM assay. (A) Electrospun silk mats were added to the CAM at embryonic day 8 (E8) and the effect on the blood vessel density was studied at E13. (B) Representative dissecting microscope images of the CAM after exposure to PBS (negative control), VEGF165 (50 ng mL^{-1}; positive control), or silk or PIII-treated silk biomaterial with or without rDV. Scaffolds are outlined by the dotted circle. Scale bar is 1 mm. Images were analyzed for the number of branch points in a size-defined area (C) and the number of blood vessels at the scaffold intersection (D). Data are expressed as fold change relative to PBS (mean $\pm$ standard deviation, $n > 5$). * denotes significant difference relative to PBS analyzed by one-way ANOVA, # denotes significant difference relative to Silk analyzed by one-way ANOVA.

time on CAM. In contrast, the PIII treated electrospun silk mats with and without biofunctionalization both exhibited a significantly ($p < 0.05$) higher number of both branch points in the area surrounding the scaffold and branches intersecting the scaffolds compared to unmodified silk, indicating that these PIII treated scaffolds were angiogenic.

4. Conclusions and future directions

This study demonstrates the potential of PIII-treated electrospun silk fibroin scaffolds biofunctionalized with recombinant perlecan domain V (rDV) for vascular graft applications. PIII treatment enhanced cell interactions non-selectively, therefore, rDV biofunctionalization is vital as it provides vascular cell selectivity. PIII treatment enabled robust and stable immobilization of rDV without affecting the mechanical properties of the bulk materials, and the rDV-biofunctionalized PIII-treated electrospun silk scaffolds demonstrated enhanced endothelial cell adhesion, proliferation, and retention under physiological flow conditions while inhibiting smooth muscle cell adhesion and proliferation. These properties are essential for promoting graft endothelialization and mitigating the risk of neointimal hyperplasia, two critical challenges in vascular graft design. Furthermore, the PIII-treated scaffolds exhibited angiogenic potential *in vivo*, underscoring their capacity to facilitate capillary ingrowth and graft integration.

The focus of this work was to evaluate the effect of PIII treatment on rDV immobilization and biofunctionality on clinically relevant electrospun silk scaffolds. Future studies will investigate the effects of PIII-immobilized rDV on complex

biological interactions and functional performance in preclinical *in vivo* models.

Data availability

Data is available from corresponding authors upon reasonable request.

Conflicts of interest

There are no conflicts to declare.

Acknowledgements

References

1 S. Jiang, S. G. Wise, J. C. Kovacic, J. Rnjak-Kovacina and M. S. Lord, Biomaterials containing extracellular matrix molecules as biomimetic next-generation vascular grafts, *Trends Biotechnol.*, 2024, **42**(3), 369–381.

2 S. Jebari-Benslaiman, U. Galicia-García, A. Larrea-Sebal, J. R. Olaetxea, I. Alloza, K. Vandenbroeck, A. Benito-Vicente and C. Martín, Pathophysiology of atherosclerosis, *Int. J. Mol. Sci.*, 2022, **23**(6), 3346.

3 W. Herrington, B. Lacey, P. Sherliker, J. Armitage and S. Lewington, Epidemiology of atherosclerosis and the potential to reduce the global burden of atherothrombotic disease, *Circ. Res.*, 2016, **118**(4), 535–546.

4 A. D. Michaels and K. Chatterjee, Angioplasty versus bypass surgery for coronary artery disease, *Circulation*, 2002, **106**(23), e187–e190.

5 T. I. Kim, Y. Zhang, J. A. Cardella, R. J. Guzman and C. I. Chaar, Outcomes of bypass and endovascular interventions for advanced femoropopliteal disease in patients with premature peripheral artery disease, *J. Vasc. Surg.*, 2021, **74**(6), 1968–1977.

6 H. J. Salacinski, S. Goldner, A. Giudiceandrea, G. Hamilton, A. M. Seifalian, A. Edwards and R. J. Carson, The mechanical behavior of vascular grafts: a review, *J. Biomater. Appl.*, 2001, **15**(3), 241–278.

7 R. M. Green, W. M. Abbott, T. Matsumoto, J. R. Wheeler, N. Miller, F. J. Veith, S. Money, H. E. Garrett and Above-Knee Femoropopliteal Study Group, Prosthetic above-knee femoropopliteal bypass grafting: five-year results of a randomized trial, *J. Vasc. Surg.*, 2000, **31**(3), 417–425.

8 P. Klinkert, P. N. Post, P. J. Breslau and J. H. Van Bockel, Saphenous vein versus PTFE for above-knee femoropopliteal bypass. A review of the literature, *Eur. J. Vasc. Endovasc. Surg.*, 2004, **27**(4), 357–362.

9 A. R. Murphy and D. L. Kaplan, Biomedical applications of chemically-modified silk fibroin, *J. Mater. Chem.*, 2009, **19**(36), 6443–6450.

10 T. Tanaka, R. Tanaka, Y. Ogawa, Y. Takagi, M. Sata and T. Asakura, Evaluation of small-diameter silk vascular grafts implanted in dogs, *JTCVS Open*, 2021, **6**, 148–156.

11 P. Gupta, K. L. Lorentz, D. G. Haskett, E. M. Cunnane, A. K. Ramaswamy, J. S. Weinbaum, D. A. Vorp and B. B. Mandal, Bioresorbable silk grafts for small diameter vascular tissue engineering applications: In vitro and in vivo functional analysis, *Acta Biomater.*, 2020, **105**, 146–158.

12 A. Settembrini, G. Buongiovanni, P. Settembrini, A. Alessandrino, G. Freddi, G. Vettor and E. Martelli, *In vivo* evaluation of silk fibroin small-diameter vascular grafts: state of art of preclinical studies and animal models, *Front. Surg.*, 2023, **10**, 1090565.

13 E. C. Filipe, M. Santos, J. Hung, B. S. Lee, N. Yang, A. H. Chan, M. K. Ng, J. Rnjak-Kovacina and S. G. Wise, Rapid endothelialization of off-the-shelf small diameter silk vascular grafts, *JACC: Basic Transl. Sci.*, 2018, **3**(1), 38–53.

14 A. H. Chan, E. C. Filipe, R. P. Tan, M. Santos, N. Yang, J. Hung, J. Feng, S. Nazir, A. J. Benn, M. K. Ng and J. Rnjak-Kovacina, Altered processing enhances the efficacy of small-diameter silk fibroin vascular grafts, *Sci. Rep.*, 2019, **9**(1), 17461.

15 V. Catto, S. Farè, I. Cattaneo, M. Figliuzzi, A. Alessandrino, G. Freddi, A. Remuzzi and M. C. Tanzi, Small diameter electrospun silk fibroin vascular grafts: Mechanical properties, in vitro biodegradability, and in vivo biocompatibility, *Mater. Sci. Eng., C*, 2015, **54**, 101–111.

16 X. Zhang, M. R. Reagan and D. L. Kaplan, Electrospun silk biomaterial scaffolds for regenerative medicine, *Adv. Drug Delivery Rev.*, 2009, **61**(12), 988–1006.

17 K. Chen, Y. Li, Y. Li, W. Pan and G. Tan, Silk fibroin combined with electrospinning as a promising strategy for tissue regeneration, *Macromol. Biosci.*, 2023, **23**(2), 2200380.

18 J. Rnjak-Kovacina, F. Tang, J. M. Whitelock and M. S. Lord, Silk biomaterials functionalized with recombinant domain V of human perlecan modulate endothelial cell and platelet interactions for vascular applications, *Colloids Surf., B*, 2016, **148**, 130–138.

19 X. Lin, F. Tang, S. Jiang, H. Khamis, A. Bongers, J. M. Whitelock, M. S. Lord and J. Rnjak–Kovacina, A biomimetic approach toward enhancing angiogenesis: recombinantly expressed domain V of human perlecan is a bioactive molecule that promotes angiogenesis and vascularization of implanted biomaterials, *Adv. Sci.*, 2020, **7**(17), 2000900.

20 H. N. Kim, Z. Elgundi, X. Lin, L. Fu, F. Tang, E. S. Moh, M. Jung, K. Chandrasekar, F. Bartlett-Tomasetig, C. Foster and N. H. Packer, Engineered short forms of perlecan enhance angiogenesis by potentiating growth factor signalling, *J. Controlled Release*, 2023, **362**, 184–196.

21 S. Jiang, N. Yang, R. P. Tan, E. S. Moh, L. Fu, N. H. Packer, J. M. Whitelock, S. G. Wise, J. Rnjak–Kovacina and M. S. Lord, Tuning Recombinant Perlecan Domain V to Regulate Angiogenic Growth Factors and Enhance Endothelialization of Electrospun Silk Vascular Grafts, *Adv. Healthcare Mater.*, 2024, **13**(23), 2400855.

22 M. S. Lord, W. Yu, B. Cheng, A. Simmons, L. Poole-Warren and J. M. Whitelock, The modulation of platelet and endothelial cell adhesion to vascular graft materials by perlecan, *Biomaterials*, 2009, **30**(28), 4898–4906.

23 K. Lau, A. Waterhouse, B. Akhavan, L. Gao, H. N. Kim, F. Tang, J. M. Whitelock, M. M. Bilek, M. S. Lord and J. Rnjak-Kovacina, Biomimetic silk biomaterials: Perlecan-functionalized silk fibroin for use in blood-contacting devices, *Acta Biomater.*, 2021, **132**, 162–175.

24 A. Kondyurin, K. Lau, F. Tang, B. Akhavan, W. Chrzanowski, M. S. Lord, J. Rnjak-Kovacina and M. M. Bilek, Plasma ion implantation of silk biomaterials enabling direct covalent immobilization of bioactive agents for enhanced cellular responses, *ACS Appl. Mater. Interfaces*, 2018, **10**(21), 17605–17616.

25 E. A. Wakelin, M. J. Davies, M. M. Bilek and D. R. McKenzie, Temperature activated diffusion of radicals through ion implanted polymers, *ACS Appl. Mater. Interfaces*, 2015, **7**(47), 26340–26345.

26 M. M. Bilek and D. R. McKenzie, Plasma modified surfaces for covalent immobilization of functional biomolecules in the absence of chemical linkers: towards better biosensors and a new generation of medical implants, *Biophys. Rev.*, 2010, **2**(2), 55–65.

27 K. Lau, L. Fu, A. Zhang, B. Akhavan, J. Whitelock, M. M. Bilek, M. S. Lord and J. Rnjak–Kovacina, Recombinant perlecan domain V covalently immobilized on silk biomaterials via plasma immersion ion implantation supports the formation of functional endothelium, *J. Biomed. Mater. Res., Part A*, 2023, **111**(6), 825–839.

28 M. Jung, M. S. Lord, B. Cheng, J. G. Lyons, H. Alkhouri, J. M. Hughes, S. J. McCarthy, R. V. Iozzo and J. M. Whitelock, Mast cells produce novel shorter forms of perlecan that contain functional endorepellin: a role in angiogenesis and wound healing, *J. Biol. Chem.*, 2013, **288**(5), 3289–3304.

29 A. Zhang, J. K. U. Wong, K. Redzikultsava, M. Baldry, S. K. H. Alavi, Z. Wang, *et al.*, A cost-effective and enhanced mesenchymal stem cell expansion platform with internal plasma-activated biofunctional interfaces, *Mater. Today Bio*, 2023, **22**, 100727.

30 E. Kosobrodova, A. Kondyurin, V. Solodko, A. S. Weiss, D. R. McKenzie and M. M. M. Bilek, Covalent Biofunctionalization of the Inner Surfaces of a Hollow-Fiber Capillary Bundle Using Packed-Bed Plasma Ion Implantation, *ACS Appl. Mater. Interfaces*, 2020, **12**(28), 32163–32174.

31 K. Redzikultsava, M. Baldry, A. Zhang, S. K. Alavi, B. Akhavan and M. M. Bilek, Cold plasma treatment of porous scaffolds: Design principles, *Plasma Processes Polym.*, 2022, **19**(7), 2200018.

32 S. G. Wise, H. Liu, A. Kondyurin, M. J. Byrom, P. G. Bannon, G. A. Edwards, A. S. Weiss, S. Bao and M. M. Bilek, Plasma ion activated expanded polytetrafluoroethylene vascular grafts with a covalently immobilized recombinant human tropoelastin coating reducing neointimal hyperplasia, *ACS Biomater. Sci. Eng.*, 2016, **2**(8), 1286–1297.

33 H. J. Jin, S. V. Fridrikh, G. C. Rutledge and D. L. Kaplan, Electrospinning Bombyx mori silk with poly (ethylene oxide), *Biomacromolecules*, 2002, **3**(6), 1233–1239.

34 X. Hu, K. Shmelev, L. Sun, E. S. Gil, S. H. Park, P. Cebe and D. L. Kaplan, Regulation of silk material structure by temperature-controlled water vapor annealing, *Biomacromolecules*, 2011, **12**(5), 1686–1696.

35 K. Shang, J. Rnjak-Kovacina, Y. Lin, R. S. Hayden, H. Tao and D. L. Kaplan, Accelerated in vitro degradation of optically clear low β-sheet silk films by enzyme-mediated pretreatment, *Transl. Vis. Sci. Technol.*, 2013, **2**(3), 2.

36 K. Lau, C. Heu, M. J. Moore, A. Zhang, B. Akhavan, S. G. Wise, M. M. Bilek, M. S. Lord and J. Rnjak-Kovacina, Effect of plasma ion immersion implantation on physiochemical and biological properties of silk towards creating a versatile biomaterial platform, *Mater. Today Adv.*, 2022, **13**, 100212.

37 I. A. Morozov, A. S. Mamaev, I. V. Osorgina, A. Y. Beliaev, R. I. Izumov and T. E. Oschepkova, Soft polyurethanes treated by plasma immersion ion implantation: Structural and mechanical properties of the surface–modified layer, *J. Appl. Polym. Sci.*, 2018, **135**(11), 45983.

38 Z. Wang, W. Chen, Z. Cui, K. He and W. Yu, Studies on photoyellowing of silk fibroin and alteration of its tyrosine content, *J. Text. Inst.*, 2016, **107**(4), 413–419.

39 D. V. Bax, A. Kondyurin, A. Waterhouse, D. R. McKenzie, A. S. Weiss and M. M. Bilek, Surface plasma modification and tropoelastin coating of a polyurethane co-polymer for enhanced cell attachment and reduced thrombogenicity, *Biomaterials*, 2014, **35**(25), 6797–6809.

40 S. Fan, Y. Zhang, H. Shao and X. Hu, Electrospun regenerated silk fibroin mats with enhanced mechanical properties, *Int. J. Biol. Macromol.*, 2013, **56**, 83–88.

41 X. Huang, S. Fan, A. I. Altayp, Y. Zhang, H. Shao, X. Hu, M. Xie and Y. Xu, Tunable structures and properties of electrospun regenerated silk fibroin mats annealed in water vapor at different times and temperatures, *J. Nanomater.*, 2014, **2014**(1), 682563.

42 B. D. Lawrence, S. Wharram, J. A. Kluge, G. G. Leisk, F. G. Omenetto, M. I. Rosenblatt and D. L. Kaplan, Effect of hydration on silk film material properties, *Macromol. Biosci.*, 2010, **10**(4), 393–403.

43 S. W. Ko, J. Y. Lee, J. Lee, B. C. Son, S. R. Jang, L. E. Aguilar, Y. M. Oh, C. H. Park and C. S. Kim, Analysis of drug release behavior utilizing the swelling characteristics of cellulosic nanofibers, *Polymers*, 2019, **11**(9), 1376.

44 E. Kon, M. Delcogliano, G. Filardo, D. Pressato, M. Busacca, B. Grigolo, G. Desando and M. Marcacci, A novel nano-composite multi-layered biomaterial for treatment of osteochondral lesions: technique note and an early stability pilot clinical trial, *Injury*, 2010, **41**(7), 693–701.

45 C. Tran, M. Yasir, D. Dutta, N. Eswaramoorthy, N. Suchowerska, M. Willcox and D. R. McKenzie, Single step plasma process for covalent binding of antimicrobial peptides on catheters to suppress bacterial adhesion, *ACS Appl. Bio Mater.*, 2019, **2**(12), 5739–5748.

46 C. D. Hodneland, Y. S. Lee, D. H. Min and M. Mrksich, Selective immobilization of proteins to self-assembled monolayers presenting active site-directed capture ligands, *Proc. Natl. Acad. Sci. U. S. A.*, 2002, **99**(8), 5048–5052.

47 L. S. Shlyakhtenko, A. A. Gall, J. J. Weimer, D. D. Hawn and Y. L. Lyubchenko, Atomic force microscopy imaging of

DNA covalently immobilized on a functionalized mica substrate, *Biophys. J.*, 1999, **77**(1), 568–576.

48 D. Ashok, J. Singh, S. Jiang, A. Waterhouse and M. Bilek, Reagent–Free Covalent Immobilization of Biomolecules in a Microfluidic Organ–On–A–Chip, *Adv. Funct. Mater.*, 2024, **34**(30), 2313664.

49 S. L. Hirsh, D. R. McKenzie, N. J. Nosworthy, J. A. Denman, O. U. Sezerman and M. M. Bilek, The Vroman effect: competitive protein exchange with dynamic multilayer protein aggregates, *Colloids Surf., B*, 2013, **103**, 395–404.

50 C. J. Wilson, R. E. Clegg, D. I. Leavesley and M. J. Pearcy, Mediation of biomaterial–cell interactions by adsorbed proteins: a review, *Tissue Eng.*, 2005, **11**(1–2), 1–8.

51 Y. Zhuang, C. Zhang, M. Cheng, J. Huang, Q. Liu, G. Yuan, K. Lin and H. Yu, Challenges and strategies for in situ endothelialization and long-term lumen patency of vascular grafts, *Bioact. Mater.*, 2021, **6**(6), 1791–1809.

52 M. Avci-Adali, G. Ziemer and H. P. Wendel, Induction of EPC homing on biofunctionalized vascular grafts for rapid in vivo self-endothelialization—a review of current strategies, *Biotechnol. Adv.*, 2010, **28**(1), 119–129.

53 A. J. Melchiorri, N. Hibino and J. P. Fisher, Strategies and techniques to enhance the in situ endothelialization of small-diameter biodegradable polymeric vascular grafts, *Tissue Eng., Part B*, 2013, **19**(4), 292–307.

54 P. F. Sánchez, E. M. Brey and J. C. Briceño, Endothelialization mechanisms in vascular grafts, *J. Tissue Eng. Regener. Med.*, 2018, **12**(11), 2164–2178.

55 J. Rnjak–Kovacina, F. Tang, X. Lin, J. M. Whitelock and M. S. Lord, Recombinant domain V of human perlecan is a bioactive vascular proteoglycan, *Biotechnol. J.*, 2017, **12**(12), 1700196.

56 L. Jeong, I. S. Yeo, H. N. Kim, Y. I. Yoon, D. H. Jang, S. Y. Jung, B. M. Min and W. H. Park, Plasma-treated silk fibroin nanofibers for skin regeneration, *Int. J. Biol. Macromol.*, 2009, **44**(3), 222–228.

57 K. Lau, L. Fu, A. Zhang, B. Akhavan, J. Whitelock, M. M. Bilek, M. S. Lord and J. Rnjak–Kovacina, Recombinant perlecan domain V covalently immobilized on silk biomaterials via plasma immersion ion implantation supports the formation of functional endothelium, *J. Biomed. Mater. Res., Part A*, 2023, **111**(6), 825–839.

58 S. Iyer, D. M. Ferreri, N. C. DeCocco, F. L. Minnear and P. A. Vincent, VE-cadherin-p120 interaction is required for maintenance of endothelial barrier function, *Am. J. Physiol.: Lung Cell. Mol. Physiol.*, 2004, **286**(6), L1143–L1153.

59 E. S. Harris and W. J. Nelson, VE-cadherin: at the front, center, and sides of endothelial cell organization and function, *Curr. Opin. Cell Biol.*, 2010, **22**(5), 651–658.

60 R. A. Hoshi, R. Van Lith, M. C. Jen, J. B. Allen, K. A. Lapidos and G. Ameer, The blood and vascular cell compatibility of heparin-modified ePTFE vascular grafts, *Biomaterials*, 2013, **34**(1), 30–41.

61 C. N. Duong and D. Vestweber, Mechanisms ensuring endothelial junction integrity beyond VE-cadherin, *Front. Physiol.*, 2020, **11**, 519.

62 L. Li, C. M. Terry, Y. T. Shiu and A. K. Cheung, Neointimal hyperplasia associated with synthetic hemodialysis grafts, *Kidney Int.*, 2008, **74**(10), 1247–1261.

63 S. O. Marx, H. Totary-Jain and A. R. Marks, Vascular smooth muscle cell proliferation in restenosis, *Circ.: Cardiovasc. Interventions*, 2011, **4**(1), 104–111.

64 M. S. Lord, C. Y. Chuang, J. Melrose, M. J. Davies, R. V. Iozzo and J. M. Whitelock, The role of vascular-derived perlecan in modulating cell adhesion, proliferation and growth factor signaling, *Matrix Biol.*, 2014, **35**, 112–122.

65 D. Gomez and G. K. Owens, Smooth muscle cell phenotypic switching in atherosclerosis, *Cardiovasc. Res.*, 2012, **95**(2), 156–164.

66 M. Liu and D. Gomez, Smooth muscle cell phenotypic diversity: At the crossroads of lineage tracing and single-cell transcriptomics, *Arterioscler., Thromb., Vasc. Biol.*, 2019, **39**(9), 1715–1723.

67 G. Cao, X. Xuan, J. Hu, R. Zhang, H. Jin and H. Dong, How vascular smooth muscle cell phenotype switching contributes to vascular disease, *Cell Commun. Signaling*, 2022, **20**(1), 180.

68 M. Cuellar, P. S. Puccini, V. A. T. Nio, N. F. Sandoval, C. Muoz-Camargo and J. C. B. Triana, (ed.), Bioreactor design for in vitro endothelialization of small diameter vascular grafts made of porcine intestinal submucosa (SIS), 2018 IX International Seminar of Biomedical Engineering (SIB), IEEE, 2018.

69 Y. Elsayed, C. Lekakou and P. Tomlins, Modeling, simulations, and optimization of smooth muscle cell tissue engineering for the production of vascular grafts, *Biotechnol. Bioeng.*, 2019, **116**(6), 1509–1522.

70 N. Li, A. P. Rickel, H. J. Sanyour and Z. Hong, Vessel graft fabricated by the on-site differentiation of human mesenchymal stem cells towards vascular cells on vascular extracellular matrix scaffold under mechanical stimulation in a rotary bioreactor, *J. Mater. Chem. B*, 2019, **7**(16), 2703–2713.

71 M. Ravi, V. Paramesh, S. R. Kaviya, E. Anuradha and F. P. Solomon, 3D cell culture systems: advantages and applications, *J. Cell. Physiol.*, 2015, **230**(1), 16–26.

72 K. P. Walluscheck, G. Steinhoff, S. Kelm and A. Haverich, Improved endothelial cell attachment on ePTFE vascular grafts pretreated with synthetic RGD-containing peptides, *Eur. J. Vasc. Endovasc. Surg.*, 1996, **12**(3), 321–330.

73 L. Chen, H. He, M. Wang, X. Li and H. Yin, Surface coating of polytetrafluoroethylene with extracellular matrix and anti-CD34 antibodies facilitates endothelialization and inhibits platelet adhesion under sheer stress, *Tissue Eng. Regener. Med.*, 2017, **14**, 359–370.

74 S. H. Hsu, I. J. Tsai, D. J. Lin and D. C. Chen, The effect of dynamic culture conditions on endothelial cell seeding and retention on small diameter polyurethane vascular grafts, *Med. Eng. Phys.*, 2005, **27**(3), 267–272.

75 E. Sho, M. Komatsu, M. Sho, H. Nanjo, T. M. Singh, C. Xu, H. Masuda and C. K. Zarins, High flow drives vascular endo-

thelial cell proliferation during flow-induced arterial remodeling associated with the expression of vascular endothelial growth factor, *Exp. Mol. Pathol.*, 2003, **75**(1), 1–1.

76 P. F. Davies, Hemodynamic shear stress and the endothelium in cardiovascular pathophysiology, *Nat. Clin. Pract. Cardiovasc. Med.*, 2009, **6**(1), 16–26.

77 T. Pennel, D. Bezuidenhout, J. Koehne, N. H. Davies and P. Zilla, Transmural capillary ingrowth is essential for confluent vascular graft healing, *Acta Biomater.*, 2018, **65**, 237–247.

78 H. W. Florey, S. J. Greer, J. Kiser, J. C. Poole, R. Telander and N. T. Werthessen, The development of the pseudoin-tima lining fabric grafts of the aorta, *Br. J. Exp. Pathol.*, 1962, **43**(6), 655.

79 C. O. Cassell, O. S. Hofer, W. A. Morrison and K. R. Knight, Vascularisation of tissue-engineered grafts: the regulation of angiogenesis in reconstructive surgery and in disease states, *Br. J. Plast. Surg.*, 2002, **55**(8), 603–610.

80 T. Watchararot, W. Prasongchean and P. Thongnuek, Angiogenic property of silk fibroin scaffolds with adipose-derived stem cells on chick chorioallantoic membrane, *R. Soc. Open Sci.*, 2021, **8**(3), 201618.